



Review

Recent Advances in the Development of Novel Iron–Copper Bimetallic Photo Fenton Catalysts

Gabriela N. Bosio¹, Fernando S. García Einschlag¹, Luciano Carlos^{2,*}  and Daniel O. Mártire^{1,*} 

¹ Instituto de Investigaciones Fisicoquímicas Teóricas y Aplicadas (INIFTA), Departamento de Química, Facultad de Ciencias Exactas, Universidad Nacional de la Plata, Consejo Nacional de Investigaciones Científicas y Técnicas (CONICET), La Plata 1900, Argentina

² Instituto de Investigación y Desarrollo en Ingeniería de Procesos, Biotecnología y Energías Alternativas, PROBIEN (CONICET-UNCo), Universidad Nacional del Comahue, Neuquén 8300, Argentina

* Correspondence: luciano.carlos@probien.gob.ar (L.C.); dmartire@inifta.unlp.edu.ar (D.O.M.)

Abstract: Advanced oxidation processes (AOPs) have been postulated as viable, innovative, and efficient technologies for the removal of pollutants from water bodies. Among AOPs, photo-Fenton processes have been shown to be effective for the degradation of various types of organic compounds in industrial wastewater. Monometallic iron catalysts are limited in practical applications due to their low catalytic activity, poor stability, and recyclability. On the other hand, the development of catalysts based on copper oxides has become a current research topic due to their advantages such as strong light absorption, high mobility of charge carriers, low environmental toxicity, long-term stability, and low production cost. For these reasons, great efforts have been made to improve the practical applications of heterogeneous catalysts, and the bimetallic iron–copper materials have become a focus of research. In this context, this review focuses on the compilation of the most relevant studies on the recent progress in the application of bimetallic iron–copper materials in heterogeneous photo-Fenton-like reactions for the degradation of pollutants in wastewater. Special attention is paid to the removal efficiencies obtained and the reaction mechanisms involved in the photo-Fenton treatments with the different catalysts.

Keywords: bimetallic catalysts; copper; heterogeneous catalysis; iron; photo-Fenton



Citation: Bosio, G.N.; García Einschlag, F.S.; Carlos, L.; Mártire, D.O. Recent Advances in the Development of Novel Iron–Copper Bimetallic Photo Fenton Catalysts. *Catalysts* **2023**, *13*, 159. <https://doi.org/10.3390/catal13010159>

Academic Editors: Gassan Hodaifa, Rafael Borja and Mha Albqmi

Received: 23 November 2022

Revised: 21 December 2022

Accepted: 4 January 2023

Published: 10 January 2023

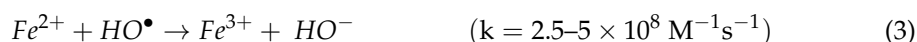
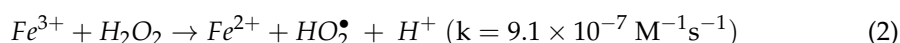
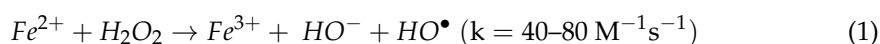


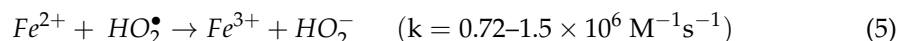
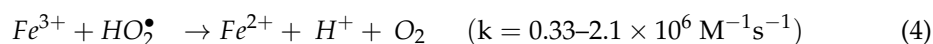
Copyright: © 2023 by the authors. Licensee MDPI, Basel, Switzerland. This article is an open access article distributed under the terms and conditions of the Creative Commons Attribution (CC BY) license (<https://creativecommons.org/licenses/by/4.0/>).

1. Introduction

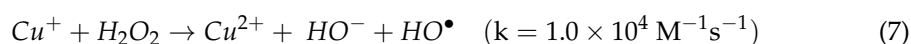
In recent years, the rapid development of the industrial sector has resulted in numerous effluents that contain toxic substances and affect the environment in a dangerous way [1]. Some of these pollutants, due to their chemical nature, are resistant to the conventional physical and biological processes commonly used in wastewater treatment plants [2]. For this reason, advanced oxidation processes (AOPs) have been postulated as viable, innovative, and efficient technologies for the removal of these compounds from water bodies [3]. Among the AOPs, the heterogeneous Fenton and photo-Fenton processes have been shown to be effective for the degradation of various types of organic compounds in industrial wastewater [4,5].

Equations (1)–(5) are the main pathways involved in the Fenton processes. Reaction 1 is a key step because it generates the strongly oxidizing radical HO^\bullet , while regeneration of Fe^{2+} is the rate-determining step under dark conditions and in the absence of alternative Fe^{3+} -reducing species (Equation (2)) [6,7].





Equations (1)–(5) are the most important steps in the dark Fenton chemistry because H_2O_2 is consumed and Fe^{2+} is regenerated from Fe^{3+} by these reactions. The HO^\bullet and HO_2^\bullet radicals are the main species involved in the oxidation of pollutants. In addition to $Fe(II)$, other transition metal ions can also promote similar processes, which are then referred to as Fenton-like or Fenton-type. For example, both oxidation states of copper can react with H_2O_2 to form HO_2^\bullet and HO^\bullet radicals (Equations (6) and (7)) [8].



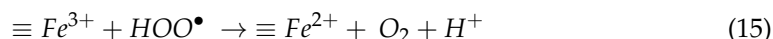
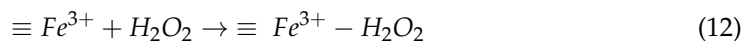
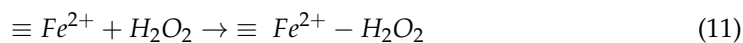
Under suitable conditions, copper can act as a better catalyst compared to iron, as it is able to form temporary complexes with oxidation products and rapidly convert Cu^+ to Cu^{2+} and vice versa [9–11]. Since the oxidation products do not form stable complexes with copper, reactive coordination sites remain available for continuous catalytic cycling. Therefore, copper not only provides a better redox cycle but is also active in the mineralization of organic matter. However, a major disadvantage of copper-based catalysts is the high excess of H_2O_2 required to maintain catalytic activity, which increases treatment costs [12]. This disadvantage has often been mitigated by the use of bimetallic composites of copper and iron [9,13–15].

Since Reaction 1 proceeds much faster than Reaction 2, the Fe^{2+} ions are consumed faster than generated, so that a large amount of ferric hydroxide is formed as sludge during the process, which causes additional problems in separation and disposal [6,16,17]. Fenton (H_2O_2/Fe^{2+}) and Fenton-like (H_2O_2/Fe^{3+}) processes can be significantly enhanced under ultraviolet (UV)/visible irradiation ($\lambda < 600$ nm). The UV region of the electromagnetic spectrum extends from about 100 nm to 400 nm, while the visible region extends from about 400 nm to 760 nm [18]. Photoirradiation prevents the accumulation of Fe^{3+} ions in the system since Fe^{2+} ions are regenerated from Fe^{3+} by photoreduction [17,19–21]. The improvement in pollutant removal rates achieved with the photo-Fenton process compared to the Fenton process can be explained by the following contributions [6,22–24]: (i) the generation of HO^\bullet and Fe^{2+} via the photolysis of iron (III) hydroxo complexes ($\lambda < 580$ nm) (Equations (8) and (9)) [25,26], followed by the participation of Fe^{2+} in Equation (1) to generate further HO^\bullet radicals [27], (ii) the photolysis of H_2O_2 when $\lambda < 310$ nm is used, and (iii) the photolysis of $Fe(III)$ chelates (Fe_3L) formed between Fe^{3+} and the organic substrate, its degradation intermediates or other ligands present in the reaction medium (Equation (10)) [6]. However, the photo-Fenton process still has some disadvantages, such as the narrow pH range (2.8–3.5), poor switching between Fe^{2+} and Fe^{3+} , and sludge formation. Therefore, many efforts have been made to develop catalysts that can operate efficiently at circumneutral pH conditions [28–31].



In the heterogeneous Fenton process, solid iron catalysts (such as the iron minerals magnetite (Fe_3O_4) or hematite ($\alpha\text{-}Fe_2O_3$)) are used instead of aqueous Fe^{2+} , to catalyze the generation of hydroxyl radicals in acidic or near-neutral media [32,33]. The mechanism of this process starts with the adsorption of H_2O_2 on the surface of Fe-based catalysts [34,35]. Then, the formation of a surface complex ($\equiv Fe^{2+}\text{-}H_2O_2$ and/or $\equiv Fe^{3+}\text{-}H_2O_2$) precursor occurs (Equations (11) and (12)). Subsequently, the $Fe^{2+}\text{-}H_2O_2$ complex generates $\equiv Fe^{3+}$ and the surface-bound HO^\bullet radical by intramolecular electron transfer (Reaction 13) [36].

The $\equiv Fe^{3+}-H_2O_2$ complex can be converted to $\equiv Fe^{2+}$ and $\bullet OOH$ (Equation (14)) [36], and the $HOO\bullet$ can further regenerate $\equiv Fe^{2+}$ (Equation (15)) [37]. The $HO\bullet$ can either attack the adsorbed organic compounds in the vicinity or oxidize the non-adsorbed organic compounds.



Monometallic iron catalysts (ZVI, Fe_2O_3 , Fe_3O_4 , and $Fe(OOH)$) are limited in practical applications due to their low catalytic activity, poor stability, and recyclability [38]. On the other hand, copper-based oxides have become the priorities of research into novel photocatalysts, due to their advantages such as strong light absorption, high carrier mobility, non-toxicity, environmental friendliness, long-term stability, and low production cost. In particular, copper has the property of a Lewis acid, which can create a localized acidic microenvironment by interacting with iron species. The effect of expanding the pH range of the system is achieved by the localized acidic microenvironment when bimetallic $Fe-Cu$ photocatalysts are used [39]. In this context, great efforts have been made to improve the practical applications of heterogeneous catalysts, and bimetallic oxides (composite oxides of iron and another metallic element) are an active research area. Similarly, bimetallic catalysts composed of iron and copper are advantageous for the reduction of Fe^{3+} in Fenton-like reactions. Previous reports have suggested that the cooperation between the redox pairs of iron (Fe^{3+}/Fe^{2+}) and copper (Cu^{2+}/Cu^+) [40,41] can accelerate electron transfer at the interface to promote the rapid reduction of Fe^{3+} . Han et al. [42] explained the synergistic effect due to the reduced ΔE for the Fe^{3+}/Fe^{2+} redox cycle obtained for the bimetallic $Fe-Cu$ catalyst compared to the monometallic Fe catalyst. Sun et al. [43] suggested that the Fe^{2+} species of the $Fe-Cu$ bimetallic catalyst is mainly regenerated by the reaction between Fe^{3+} and Cu^+ (Equation (16)) rather than by the reduction of Fe^{3+} by H_2O_2 (Equation (2)). Thus, the coexistence of Fe and Cu on the surface of a catalyst can accelerate the process of electron transfer in the reaction environment and create a suitable condition for the generation of reactive radical species.



In summary, for the above reasons, bimetallic iron-copper materials are likely to perform better as heterogeneous Fenton and photo-Fenton catalysts compared to monometallic iron or copper materials. In this context, this review focuses on the compilation of the most relevant studies on the recent advances in the application of bimetallic iron-copper materials as Fe and Cu sources in heterogeneous photo-Fenton-like reactions for the degradation of pollutants in wastewater. Although the differences in the model pollutants and the experimental conditions make an evaluation difficult, we used as central parameters for the comparisons between the different materials, on the one hand, the combinations "achieved efficiency/treatment time" (which can be found in the tables) and, on the other hand, the dominant mechanisms in each study. For clarity, the results in the next sections are classified into the following groups according to the chemical composition of the catalysts (Figure 1): (i) $CuFe_2O_4$, (ii) mixed ferrites containing Fe and Cu , (iii) $CuFeO_2$ and $CuFeS_2$ materials, (iv) $Fe-Cu$ oxide composites, (v) Metal-Organic Frameworks (MOF) based on Fe and Cu .

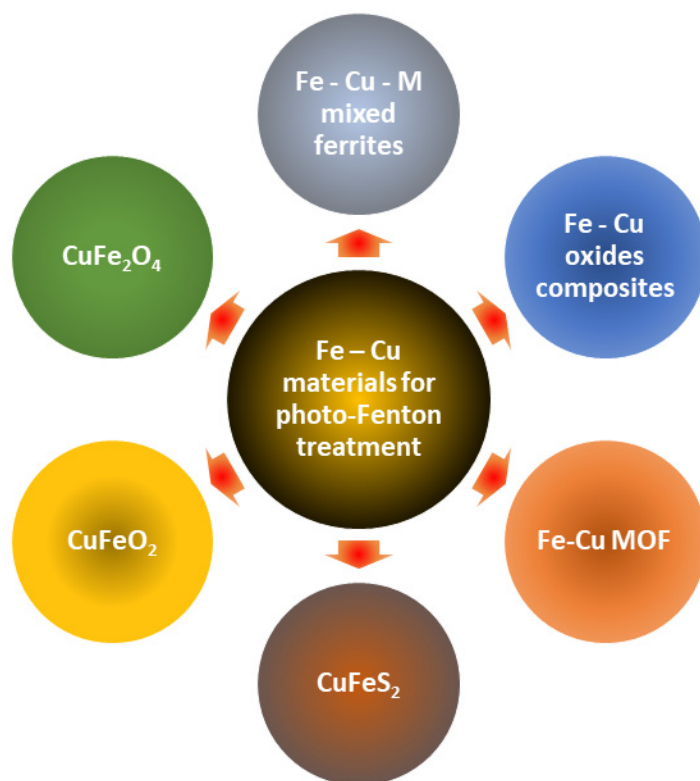


Figure 1. Classification of the different Fe–Cu based materials applied as catalysts in photo-Fenton processes.

2. CuFe_2O_4

Ferrites are a broad class of iron-bearing oxides that include spinel ferrites, perovskites, ilmenite (FeTiO_3), and hexagonal ferrites (or hexaferrites). In general, spinel ferrites can be described as ferrites with the formula $M\text{Fe}_2\text{O}_4$, where M is a divalent metal cation (such as Fe , Co , Zn , Ni , Cu , or others) [44]. Due to their thermal stability [45], unique structural [46], optical [47], magnetic [48], electrical, and dielectric properties [49], spinel ferrites have broad potential technological applications in photoluminescence [50], photocatalysis [51], biosensor development [52], magnetic drug delivery [53], corrosion protection [54], antimicrobial agents [55], and biomedicine (hyperthermia) [56]. In particular, CuFe_2O_4 has an inverse spinel structure with 8 Cu^{2+} ions in octahedral sites and 16 Fe^{3+} ions evenly distributed between the tetrahedral (A) and octahedral (B) sites [57].

The Tauc's equation was used to determine the optical band gap (E_g) of copper ferrite [58]:

$$\alpha h\nu = B(h\nu - E_g)^m$$

where α is the energy-dependent absorption coefficient, $h\nu$ is the photon energy, B is an energy independent constant, and the factor m depends on the nature of the electron transition and is equal to 2 or 1/2 for the direct and indirect transition band gaps, respectively. Assuming a direct semiconductor, E_g can be obtained from the extrapolation of the linear section of Tauc's plot of $(\alpha h\nu)^{0.5}$ vs. $h\nu$ to the energy axis. In comparison with other spinel ferrites such as CoFe_2O_4 ($E_g = 2.7$ eV) and NiFe_2O_4 NPs ($E_g = 2.2$ eV) [59], CuFe_2O_4 NPs have a relatively small band gap of (1.7–1.9 eV) which allows them to use freely available energy in the form of sunlight to degrade pollutants in water [59]. Since CuFe_2O_4 is a narrow band gap material, it can be successfully used in type II or Z-scheme heterojunction photocatalysts [60].

Wei et al. [39] prepared magnetic Fe–Cu materials by the sol–gel method. Solutions containing 0–40% Cu^{2+} were prepared separately to obtain catalysts with different iron and copper ratios. The molar ratio of iron and copper had significant effects on the surface

and structural properties of the materials. These materials were used for the removal of pyridine under UV irradiation in a Fenton-like system. The effects of various parameters, such as the molar ratio of *Fe* and *Cu*, catalyst and H_2O_2 dosage, initial pH, and initial pyridine concentration were studied. The best degradation performance was obtained for the M-40% material prepared from the 40% Cu^{2+} solution, which consisted of Fe_2O_3 and $CuFe_2O_4$. This co-doped *Fe*-*Cu* catalyst showed high activity, good stability, and easy recovery for the degradation of pyridine when the catalyst loading was 0.90 g L^{-1} , the H_2O_2 dosage was 832.50 mg L^{-1} , the initial pH was 7, and the initial pyridine concentration was 100.00 mg L^{-1} . The degradation efficiency of pyridine was more than 99% within 30 min and the TOC removal efficiency was 97.4% within 50 min. Therefore, the M-40% catalyst could be a potential material for wastewater treatment, which could extend the active pH range to facilitate recycling and reuse. The proposed reaction mechanism involves the reduction of Cu^{2+} to Cu^+ at the surface of the photocatalyst (Equation (6)), and the reaction of Cu^+ with H_2O_2 to form hydroxyl radicals and Cu^{2+} (Equation (7)). In addition, HO^\bullet is obtained from Cu^{2+} and water under UV irradiation (Equation (17)). Part of Cu^{2+} is reduced to Cu^+ by $O_2^{\bullet-}$ according to Equation (18). Furthermore, the monovalent copper ions can also be oxidized by H_2O_2 to produce Cu^{3+} , which reacts with water molecules under UV light to form hydroxyl radicals (Equations (19) and (20)). Direct evidence for the occurrence of Equation (19) was obtained by EPR spectroscopy using the spin-trapping approach [61]. It is very likely that this reaction occurs at the surface of the photocatalyst. The complete mechanism is shown in Figure 2.

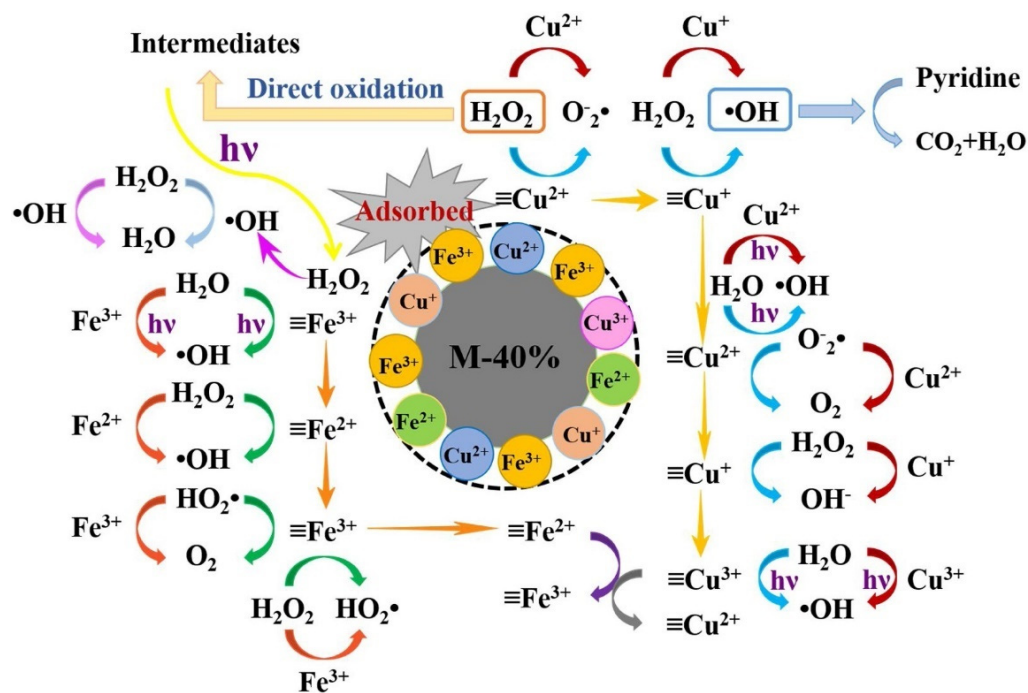
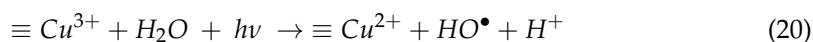
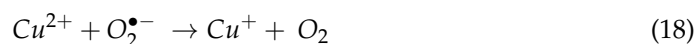
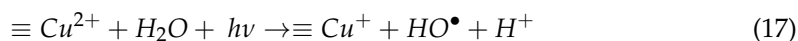


Figure 2. Reaction mechanism proposed for the degradation of pyridine by the UV/M-40%/H₂O₂ system. Reprinted with permission from Ref. [39]. Copyright 2020, Elsevier.

Silva et al. [62] prepared mixed iron and copper oxides by the modified Pechini's method. The samples were calcined at different temperatures and used for the removal of Methylene Blue dye (MB) by solar photo-Fenton catalysis. The results of X-ray diffraction analysis showed that hematite and copper ferrite phases were mainly responsible for the high efficiency of the photochemical reaction. MB removal from the aqueous solution was carried out in the presence of H_2O_2 (300 mg L^{-1}), with a 1.0 g L^{-1} catalyst, at a neutral pH, and under solar irradiation. One of the catalysts was more efficient than pure iron (Fe_2O_3) and copper oxides (CuO), indicating the synergistic effect produced by combining the two metals on the same material. The authors proposed a mechanism for the regeneration of the active sites that satisfactorily explained the experimental results.

Cao et al. [63] prepared $CuFe_2O_4$ composites via combustion solution synthesis. The authors studied the effect of Cu content on the synthesized composites. The composite with 18 wt.% Cu had the best photo-Fenton activity. This nanocomposite, which was composed of $CuFe_2O_4$ and CuO , could degrade 40 mg L^{-1} MB, 20 mg L^{-1} Rhodamine B (RhB), and 20 mg L^{-1} methyl orange (MO) in 40, 30, and 50 min, respectively. In addition, the composite showed superparamagnetic behavior and could be recycled.

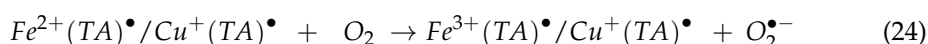
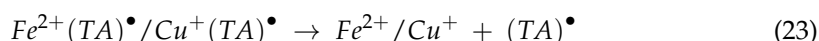
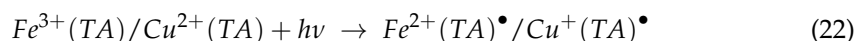
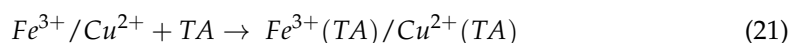
Guo et al. [40] synthesized self-assembled hollow nanospheres of $CuFe_2O_4$ using the solvothermal method. The catalytic activity of the nanospheres was evaluated by the degradation of MB. In addition, these authors compared the properties of $CuFe_2O_4$ particles prepared by different methods. It was found that the good performance of the solid catalyst depends on both the large specific surface area and the degree of the optical response. The increase in photoelectric response and conductivity are beneficial for the improvement of catalytic performance. Transient photo-current experiments showed that the samples obtained by the solvothermal method exhibited a better optical response in the on-off cycle under light conditions.

Leichtweis et al. [64] prepared a novel composite catalyst by doping $CuFe_2O_4$ nanoparticles in the malt bagasse biochar. Malt bagasse (the malted barley residue) is the main residue obtained in the manufacture of beer. Composites with different ratios of malt biochar and $CuFe_2O_4$ were produced. The composites had lower band gap energy than $CuFe_2O_4$, which increased the photocatalytic activity. At 60 min of heterogeneous photo-Fenton treatment (pH 3), visible light tests showed that pure $CuFe_2O_4$ removed only 39% of the RhB color, while the composites removed up to 88% of the dye. A total of 100% color removal (pH 3) was achieved at 10- and 20-min reaction times for 10 and 50 mg L^{-1} of dye under solar irradiation. Tests performed in the presence of specific radical scavengers showed that HO^\bullet , $O_2^{\bullet-}$, and h^+ were the predominant reactive species involved in the degradation of the dye.

Jiang et al. [65] prepared a magnetic $Bi_2WO_6/CuFe_2O_4$ catalyst to be used in the removal of the antibiotic tetracycline hydrochloride (TCH). The obtained catalyst achieved 92.1% TCH (20 mg L^{-1}) degradation efficiency in a photo-Fenton-like system and a mineralization performance of 50.7% and 35.1% for TCH and a raw secondary effluent from a wastewater treatment plant, respectively. The excellent performance was attributed to the fact that photogenerated electrons accelerated the conversion $Fe(III)/Fe(II)$ and $Cu(II)/Cu(I)$, which increased the reaction rates of $Fe(II)/Cu(I)$ with H_2O_2 and generated abundant HO^\bullet radicals for pollutant oxidation. EPR assays confirmed that $O_2^{\bullet-}$ and HO^\bullet were mainly responsible for THC degradation in dark and photo-Fenton-like systems, respectively.

The low efficiency of photo-Fenton processes at a neutral pH is mainly due to the precipitation of iron and can therefore be prevented by the proper addition of iron complexing agents, such as tartaric acid [66]. Guo et al. [67] prepared $CuFe_2O_4$ particles by the sol-gel method and investigated the effects of tartaric acid (TA) on the degradation of MB in the presence of $CuFe_2O_4$ and H_2O_2 under light irradiation. The results showed that the introduction of TA increased the decolorization rate of MB decolorization from 52.0% to 92.1% within 80 min. The contribution of $O_2^{\bullet-}$ was only 10%, whereas that of HO^\bullet was about 88%. The enhancement of MB degradation in the presence of TA was explained by the complexation of Fe^{3+} and Cu^{2+} with TA (Equation (21)), followed by a

photo-induced ligand to metal charge transfer process (Equation (22)). In the literature, similar equations with iron species and other organic radicals have been proposed to explain the photo-Fenton mechanism [66]. The photo-induced intramolecular charge transfer of the copper (II) complex of tartaric acid has already been described in the mechanism of the catalytic reduction of Cr(VI) by tartaric acid under the irradiation of simulated sunlight [68]. The excited species $Fe^{2+}/Cu^{+}-(TA)^{\bullet}$ further produced Fe^{2+}/Cu^{+} and TA^{\bullet} radicals according to Equation (23). Moreover, the presence of molecular oxygen also accelerated the transformation of the chemical state of the metal ions (see Equation (24)).



Rocha et al. [69] prepared $CuFe_2O_4$ from copper recycled from spent lithium-ion batteries. The photocatalytic properties were analyzed by monitoring the decolorization of MB in a heterogeneous photo-Fenton process in the presence of solar radiation. The decolorization efficiency was 96.1% in 45 min of reaction. Formic and acetic acids were detected as degradation products of MB by ion chromatography.

Lin and Lu [70] developed $CuFe_2O_4$ nanoparticles decorated on partially reduced graphene oxides ($CuFe_2O_4@rGO$), to selectively and efficiently cleave lignin model compounds into value-added aromatic chemicals via a sunlight-assisted heterogeneous Fenton process. Controlled oxidative cleavage of the lignin model compound enabled the production of high-value aromatic chemicals, guaiacol and 2-methoxy-4-propylphenol, in high yields, instead of complete mineralization of the lignin model compound. The partially reduced graphene oxides serve as the large size support to accommodate and immobilize the $CuFe_2O_4$ nanoparticles for easy recycling of the catalyst, to attract the lignin model compounds through π - π stacking and hydrogen bonding for efficient cleavage reaction, and to accelerate the transport of photo-induced electrons for better charge separation and thus higher photocatalytic activities.

Membrane separation offers many advantages in wastewater treatment, including high efficiency, low energy consumption, and ease of operation [71]. However, membrane fouling always lowers the separation efficiency and shortens the membrane life, which greatly hinders the application of membrane technology. For this reason, Wang et al. [72] combined photo-Fenton and membrane processes for water treatment (Figure 3). These authors synthesized $CuFe_2O_4$ particles and doped them into the $PVDF@CuFe_2O_4$ membranes. The photo-Fenton process can degrade various foulants through the generation of hydroxyl radicals, which improves the filtration performance of the membranes.

The $PVDF@CuFe_2O_4$ membrane (1.0% $CuFe_2O_4$) showed significant improvement in both permeability and separation, with a tripling of flux and doubling of rejection compared to the values obtained by the membrane filtration process itself. In addition, the $PVDF@CuFe_2O_4$ nanofiltration membrane showed excellent stability and reusability after repeated tests over fifteen cycles.

Recently reported studies on the use of $CuFe_2O_4$ as photo-Fenton photocatalysts are summarized in Tables below.

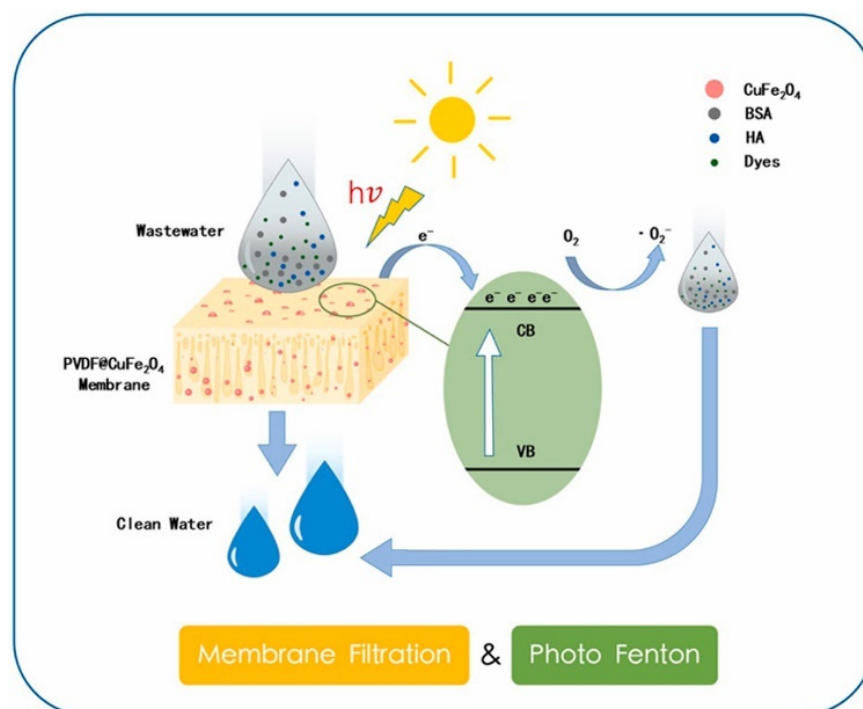


Figure 3. Schematic diagram illustrating the integration system of membrane filtration and the photo-Fenton process. BSA: bovine serum albumin; HA: humic acid. Reprinted with permission from Ref. [72]. Copyright 2019, Elsevier.

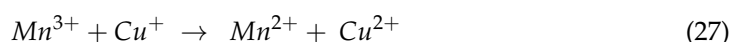
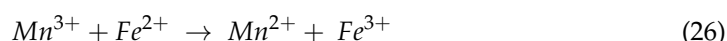
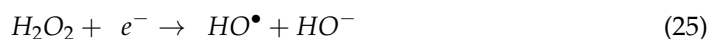
3. Mixed Ferrites Containing Fe and Cu

As already mentioned, among the iron-based materials used as heterogeneous photo-Fenton catalysts, ferrites have attracted much attention because they are chemically and thermally stable magnetic materials [73,74]. Most importantly, ferrites have a narrow band gap, which enables them to efficiently utilize the visible region of solar energy in photocatalysis [75]. $MnFe_2O_4$ has a large specific surface area, good biocompatibility, and excellent magnetic properties [76,77]. However, mixed ferrites have better catalytic behavior compared to single ferrites [78]. In particular, doping with Cu^{2+} could improve the optical properties of $MnFe_2O_4$, which is due to the lattice defects in the spinel structure generated as a consequence of the smaller ionic radius of Cu^{2+} . In addition, doping with other metals can also introduce oxygen vacancies, leading to a significant improvement in catalytic performance due to structural distortions [79]. Meena et al. [80] prepared Ce-doped $MnFe_2O_4$ by a low-temperature solution combustion synthesis using Oxalyl Dihydrazine (ODH) as fuel and reported that the band gap decreased after Ce-doping compared to that of pure $MnFe_2O_4$. Moreover, copper, manganese, and iron have been shown to have synergistic effects [81]. Thus, Cu^{2+} -doped $MnFe_2O_4$ could further improve the catalytic activity because the different radii of metal ions in the spinel structure may lead to some defects and distortions, which result in the production of reactive oxygen species (ROS) [82].

Yang et al. [83] synthesized porous $Cu_{0.5}Mn_{0.5}Fe_2O_4$ nanoparticles by a co-precipitation process and a subsequent high-temperature annealing treatment method. $Cu_{0.5}Mn_{0.5}Fe_2O_4$ nanoparticles exhibited much higher catalytic activity towards the degradation of bisphenol A (BPA) by the activation of H_2O_2 under UV light irradiation compared with $CuFe_2O_4$ and $MnFe_2O_4$ nanoparticles. The authors proved, through radical scavenger and EPR/DMPO experiments, that the hydroxyl radical is involved and plays a critical role in the presence of H_2O_2 . They also proposed a possible BPA degradation pathway.

Sun et al. [82] employed $Cu_{0.8}Mn_{0.2}Fe_2O_4$ in the presence of H_2O_2 and achieved a great improvement in the degradation efficiency of TCH, which was due to the fact that H_2O_2 was activated by the Fe, Mn, and Cu ions on the $Cu_{0.8}Mn_{0.2}Fe_2O_4$ surface to

generate HO^\bullet radicals. Two possible mechanisms for H_2O_2 activation by $Cu_{0.8}Mn_{0.2}Fe_2O_4$ at pH = 3 and pH = 11 were proposed. Firstly, $Cu_{0.8}Mn_{0.2}Fe_2O_4$ could be excited by visible light to generate electrons (e^-) and holes (h^+), then H_2O_2 could react with the generated e^- to produce HO^\bullet (Equation (25)). Photoelectrons migrating to the surface of the catalyst immediately react with the metal ions of the catalyst, which not only promotes the circulation of Fe , Mn , and Cu components but also strengthens the synergistic effect between them (Equations (16), (26) and (27)). When H_2O_2 came into contact with Fe , Mn , and Cu ions, the Fenton reaction was triggered immediately and TCH was mineralized by these reactive species into small molecule compounds.



Wang et al. [84] used a p–n heterostructured nano–photocatalyst based on the p–type Cu_2ZnSnS_4 (CZTS) nanosheets, which were successfully assembled on the surface of $ZnFe_2O_4$ (ZFO) nanospheres, forming CZTS/ZFO p–n heterostructures. These p–n heterostructures could not only efficiently expand the spectral response and promote photo–induced charge separation, but also increase the specific surface areas for photocatalytic and photo–Fenton reactions. All these factors resulted in the p–n hetero–structured CZTS/ZFO nano–photocatalyst with significantly enhanced photocatalytic activity for the degradation of MO in the presence of H_2O_2 with visible light irradiation, compared to pure ZFO. This behavior was due to the synergistic enhancement effects of the CZTS/ZFO p–n heterostructure combined with the photo–Fenton mechanism. (Figure 4).

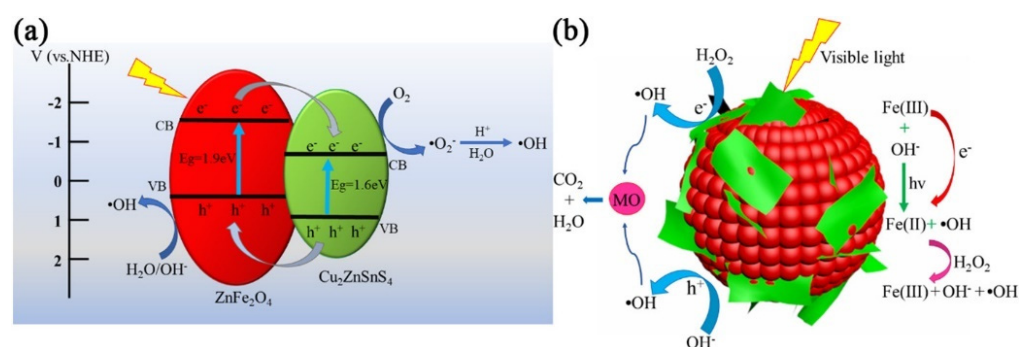


Figure 4. Schematic diagram for the photocatalytic degradation of MO by CZTS/ZFO p–n heterostructure plus H_2O_2 : (a) the energy band structure, and the photo–induced carrier separation and transfer and (b) possible mechanism of photo–Fenton reaction in CZTS/ZFO + H_2O_2 photocatalytic system. Reprinted with permission from Ref. [84]. Copyright 2020, Elsevier.

Shi et al. [85] fabricated a multi–functional honeycomb ceramic plate by coating a layer of $CuFeMnO_4$ on the surface of a cordierite (magnesium iron aluminum cyclosilicate) material. The honeycomb structure was beneficial for light trapping and energy recycling and thus improved the solar–to–water evaporation efficiency. The $CuFeMnO_4$ coating layer acted as both the photothermal material for the solar–driven water evaporation process and the catalyst for the removal of volatile organic compounds (VOCs) via the heterogeneous photo–Fenton reaction. With the integration of the photo–Fenton reaction into the solar distillation process, clean distilled water was produced with efficient removal of the potential VOCs from the contaminated water sources.

All the results described in this section are summarized in Table 1.

Table 1. Summary of recently used Fe–Cu ferrites and mixed ferrites as photo–Fenton photocatalysts in wastewater treatment.

Material ^(a)	Conditions	Contaminant	Degradation Efficiency	Reference
$Fe_2O_3/CuFe_2O_4$ ^(b)	UV light, pH 7, $[H_2O_2] = 832.50 \text{ mg L}^{-1}$	Pyridine (100 mg L^{-1})	>99% within 30 min; TOC removal of 97% within 50 min	[39]
$\alpha\text{-}Fe_2O_3/CuFe_2O_4$ ^(c)	Natural solar light, pH 7, $[H_2O_2] = 300 \text{ mg L}^{-1}$	MB (MB, 100 mg L^{-1})	100% removal of the dye in 180 min	[62]
$CuFe_2O_4/CuO$ ^(d)	Halogen lamp, pH not indicated, $[H_2O_2]$ not indicated	MB (40 mg L^{-1}), Rhodamine B (20 mg L^{-1}), Methyl Orange (20 mg L^{-1})	100% dye degradation within 50 min	[63]
Hollow $CuFe_2O_4$ nanospheres ^(e)	300-W UV curing lamp ($\lambda > 400 \text{ nm}$), pH not indicated, $[H_2O_2] = 0.02 \text{ M}$	MB (30 mg L^{-1})	96.4% in 60 min	[40]
$CuFe_2O_4$ /biochar nanocomposites ^(f)	Fluorescent lamp (395–580 nm)/Sunlight, pH 3–7, $[H_2O_2]$ from 2.5 to $10 \mu\text{M}$	Rhodamine B	100% color removal was obtained at 10 and 20 min of reaction for 10 and 50 mg L^{-1} of dye with solar radiation	[64]
$Bi_2WO_6/CuFe_2O_4$ ^(e)	Visible light, pH 2.6–6.3, $[H_2O_2] = 10 \text{ mM}$	Tetracycline hydrochloride (TCH)	After 30 min, 92.1% TCH (20 mg L^{-1}) degradation (pH 2.6) efficiency and 50.7% and 35.1% mineralization performance.	[65]
$CuFe_2O_4$ /tartaric acid (TA) ^(b)	UV-curing lamp (365–450 nm), pH 5.0, $[H_2O_2] = 0.02 \text{ M}$	MB (50 mg L^{-1})	Introducing TA enhanced MB decolorization rate from 52.0% to 92.1% within 80 min.	[67]
$CuFe_2O_4$ ^(f)	Sunlight, pH 7.0, $[H_2O_2] = 0.3 \text{ M}$	MB (10 mg L^{-1})	Decolorization efficiency was 96.1% in 45 min of reaction.	[69]
$CuFe_2O_4@rGO$ ^(g)	Simulated sunlight, pH not indicated	Guaiacylglycerol- β -guaiacyl ether (lignin model compound)	Yields of 72.6% and 52.5% were achieved for guaiacol and 2-methoxy-4-propylpheno, respectively, in 60 min.	[70]
$CuFe_2O_4$ nanoparticles doped in polyvinylidene fluoride (PVDF) membranes ^(h)	Xe arc lamp, pH 3.0–11.0. The H_2O_2 (30 wt.%) dosage was in the range 50–1200 μL in 50 mL MB solution	MB (100 mg L^{-1})	MB was thoroughly degraded in 30 min when the pH is 3.0, while there is still 15.6% of the MB left at solution pH of 11.0.	[72]
$Cu_{0.5}Mn_{0.5}Fe_2O_4$ ⁽ⁱ⁾	$Cu_{0.5}Mn_{0.5}Fe_2O_4$ 0.08 g L^{-1} pH: 4.2 $[H_2O_2] = 10 \text{ mM}$	BPA (10 mg L^{-1})	100% degradation and 47.6% mineralization 5 min	[83]
$Cu_{0.8}Mn_{0.2}Fe_2O_4$ ^(e)	Catalyst 0.100 g L^{-1} pH 3 and 11 300 W Xe lamp with a 420 nm UV-cut off filter	TC–HCL 100 mL 80 mg L^{-1}	99% 30 min	[82]
CZTS/ZFO p–n heterostructures ^(e)	Catalyst 0.5 g L^{-1} pH 3 to 9 $[H_2O_2] = 10 \text{ mM}$. 500 W Xe high intensity discharge lamp > 450 nm	MO 10 mg L^{-1}	91% 120 min At optimum pH: 6	[84]
$CuFeMnO_4$ on the surface of a honeycomb ceramic substrate ⁽ⁱ⁾	0.05g of catalyst pH = 6.71. $[H_2O_2]$ from 0 to 0.1 M Solar light	Phenol as a VOC model 10, 20,50 and 100 mg L^{-1} MB 10 mg L^{-1}	~99.18% COD and MB was removed 20 min	[85]

(a) The synthesis method is shown in the footnotes. (b) Sol–gel method. (c) Modified Pechini method. (d) Solution combustion synthesis method. (e) Solvothermal method. (f) Co–precipitation. (g) Solvent–assisted interfacial reaction process. (h) Non–solvent induced phase separation method. (i) Chemical co–precipitation method followed by high–temperature annealing treatment. (j) See original papers for detail.

4. CuFeO₂ and CuFeS₂ Materials

Bimetallic Cu(II) and Fe(II) oxides and sulfides capable of activating H₂O₂ for the degradation of organic pollutants have become a focus of research. Among these catalysts, CuFeO₂ has gained wide concern due to its simple synthesis, low cost, interesting catalytic activity, and high chemical stability. In addition, due to its narrow band gap and cooperative impact of Fe³⁺/Fe²⁺ and Cu²⁺/Cu⁺ redox cycles, CuFeO₂ materials usually exhibit significant visible–light absorption and a good performance for H₂O₂ activation.

Schmachtenberg et al. [86] obtained delafossite–type powders by conventional hydrothermal (CuFeO₂) and microwave–assisted hydrothermal (CuFeO₂–MW) routes. Both materials were tested as potential catalysts in the photo–Fenton reaction under visible light. An experimental design was used for optimizing the degradation efficiency of the dye Reactive Red 141 and assessing the effects of the operating variables pH, catalyst loading, and oxidant concentration. Both a substantial reduction in the treatment times and a significant efficiency improvement were observed for the catalyst prepared by microwave irradiation (i.e., about 98% of dye degradation at 30 min) in comparison with the material obtained by the conventional method (i.e., 84% at 150 min). The latter difference was ascribed to the fact that CuFeO₂–MW samples presented higher values of surface area and pore volume, as well as smaller band–gap energy in comparison with conventional CuFeO₂. In addition, under optimal conditions (i.e., pH = 3.0, [CuFeO₂–MW] = 0.25 g L^{−1}, and [H₂O₂] = 8 mmol L^{−1}) 80% of TOC removal was achieved at 180 min. Finally, reusability tests conducted with the CuFeO₂–MW catalyst showed only a marginal loss of decolorization efficiency after four cycles (from 98% to 93%) and total concentrations of leached Fe and Cu ions of less than 1.0 wt.% of the catalyst content.

Liu et al. [87] prepared stoichiometric CuFeO₂ microcrystals with high crystallinity and single crystal phase via the optimized hydrothermal process. The authors presented a detailed characterization including the analysis of crystal structure, optical properties, and photoelectrochemical behavior. TCH was used as a model compound to evaluate the activity of CuFeO₂ under different conditions. Since the microcrystals showed a nonnegligible photocatalytic activity in the absence of H₂O₂, the authors proposed that the photo–generated electrons in the CB of CuFeO₂ could interact with dissolved oxygen and the photo–generated holes in the valence band react with H₂O, thus forming active radicals such as O₂^{•−} and HO[•], respectively. On the other hand, in the presence of H₂O₂, the material showed some catalytic activity for the Fenton reaction under dark conditions, which was enhanced more than four times upon illumination. The heterogeneous photo–Fenton–like treatment of TCH, carried out at pH 8 and using a Xe–Lamp in a quartz cell, showed conversion degrees of about 80 and 90% within the first 60 and 120 min, respectively. Photo–Fenton assays performed in the presence of different radical scavengers indicated that HO[•] is not directly responsible for the degradation, but that the photogenerated holes and O₂^{•−} are the predominant reactive species.

Da Silveira Salla et al. [88] evaluated the catalytic properties of CuFeS₂–MW through BPA degradation tests conducted at a near–neutral pH and using simulated visible light. Results showed a remarkable enhancement of the catalytic efficiency (i.e., about 90% in the first 15 min) for the catalyst obtained in the presence of citrate, with a rate about 10 times faster than that of CuFeS₂ prepared without citrate. This behavior suggested that the presence of citric acid accelerates the photo–conversion of Fe³⁺ to Fe²⁺, thus increasing the generation of HO[•] and the efficiency of the overall process. Reusability assays showed that, after the fourth cycle, the degradation rate remained higher than 95% and the TOC decrease was 76.6% after 60 min of reaction. In addition, concentrations of Fe and Cu leached into the solution were lower than 0.5% of the total amounts of Fe and Cu present in the catalyst at the beginning of the reaction. To assess the main reactive species, tests were conducted in the presence of different ROS scavengers (i.e., t–butanol for HO[•] and p–benzoquinone for O₂^{•−}). Results showed that BPA degradation may be ascribed to the generation of HO[•]. As expected, due to the low selectivity of the HO[•] radicals, the degradation efficiency was affected by the presence of other chemical species in the real effluent such as carbonates/bicarbonates, nitrates/nitrites, sulfates, phosphates, and

chlorides. Using LC–MS analysis, the authors identified several hydroxylated derivatives resulting from the initial reaction stages. These primary intermediates are likely to undergo ring–opening reactions to form typical aliphatic acids as degradation by–products, which may further undergo a series of oxidation steps that finally lead to complete mineralization.

More recently, Da Silveira Salla et al. [89] prepared a chalcopyrite powder by a microwave–assisted method ($CuFeS_2$ –MW), which exhibited higher catalytic activity than that obtained with the material prepared by the conventional method ($CuFeS_2$). Both materials were synthesized in the presence of citric acid, which is capable of enhancing the photoreduction of $Fe(III)$. Tartrazine dye was used as a model compound for the degradation by the photo–Fenton reaction under visible irradiation at pH 3.0. $CuFeS_2$ –MW reached 99.1% of tartrazine decolorization at 40 min and 87.3% of mineralization at 150 min, the decolorization rate being twice as fast as that obtained with $CuFeS_2$. The latter difference was attributed to the synergy between higher crystallinity and increased amount of Fe^{2+} on the $CuFeS_2$ –MW surface when compared to $CuFeS_2$. Reusability tests performed on both $CuFeS_2$ –MW and $CuFeS_2$ showed that, after five cycles, the decolorization efficiencies remained at 93.6 and 69.6%, respectively. Moreover, the highest concentrations of leached iron were less than 1% of the total amount of iron present in the catalysts. The addition of t–butanol decreased 20–fold the tartrazine decolorization rate, while p–benzoquinone did not inhibit tartrazine decolorization. These results show that HO^\bullet radicals are the key species for tartrazine removal and that $O_2^{\bullet-}$ radicals do not play a significant role in the degradation mechanism.

Cai et al. [90] anchored $CuFeO_2$ on a Manganese residue (MR) through mechanical activation (MA) for obtaining Fe – $Cu@SiO_2$ /starch–derived carbon composites. The material was tested as a heterogeneous catalyst for the photo–Fenton treatment of TC using H_2O_2 and visible light. Under optimal conditions (i.e., 15 mM of H_2O_2 and pH 7.0) 100% of TC conversion (50 mg L^{-1}) was achieved within 40 min. Moreover, the observed decay constants were 4.00, 2.77, and 2.14 times higher than those of Cu/SC , $MAMR$ – $Fe_3O_4@SiO_2/SC$, and MR – Fe – $Cu@SiO_2/SC$, respectively. Reutilization tests showed good material stability since the photocatalytic performance of $MAMR$ – Fe – $Cu@SiO_2/SC$ changed from 99.2% to 96.3% after five cycles and metal leaching was below 0.1 mg L^{-1} for Cu , Fe , and Mn . Based on XPS analyses before and after material usage, the authors proposed that the efficiency of the prepared catalyst is closely related to the interaction of Cu^{2+}/Cu^+ , Fe^{3+}/Fe^{2+} , and Mn^{3+}/Mn^{2+} couples. The study of reactive species through the use of scavengers and ESR showed that both HO^\bullet and $O_2^{\bullet-}$ contribute to TC degradation in the $MAMR$ – Fe – $Cu@SiO_2/SC + H_2O_2 +$ visible light system, while surface photogeneration of electrons and holes seems to play a negligible role.

Xin et al. [38] synthesized $CuFeO_2$ /biochar composites for heterogeneous photo–Fenton–like processes (HPF–like) via the hydrothermal method. Biochar prevented agglomeration and avoided the usage of added reductants. Moreover, the introduction of biochar had several advantages, such as enhancing visible–light absorption, narrowing the bandgap of $CuFeO_2$, and partially suppressing the recombination between photoelectron and hole pairs. By applying the design of experiments and the surface response methodology the authors studied the effects of the operating conditions on TC degradation efficiency. The results showed that the optimum parameters were 220 mg L^{-1} of catalysts, 22 mM of H_2O_2 , and pH 6.4, with a pH dependence relatively gentle in the range of 4.0 to 8.0. Under optimal conditions, the efficiency of TC degradation in HPF–like systems was 96.7% after 120 min of treatment. Furthermore, the catalyst exhibited excellent stability since the activity only decreased by 3.9% after five utilization cycles and the total dissolved concentrations of both iron and copper ions at 120 min were below 0.02 mg L^{-1} . Active species scavenging experiments were carried out by using p–benzoquinone, silver nitrate, methyl alcohol, and ammonium oxalate as the scavengers of $O_2^{\bullet-}$, photoelectrons, HO^\bullet , and photogenerated holes, respectively. Interestingly, ammonium oxalate did not decrease the catalytic performance but accelerated the TC degradation rate. The latter effect was attributed to a lower photoelectron quenching rate, which could promote Fe^{3+}/Fe^{2+} and Cu^{2+}/Cu^+ cycles,

thus significantly improving H_2O_2 activation. In addition, ESR experiments allowed the identification of HO^\bullet as the predominant active species, whereas photoelectrons and $O_2^{\bullet-}$, were auxiliary species for TC degradation. The mechanistic findings are schematically summarized in Figure 5.

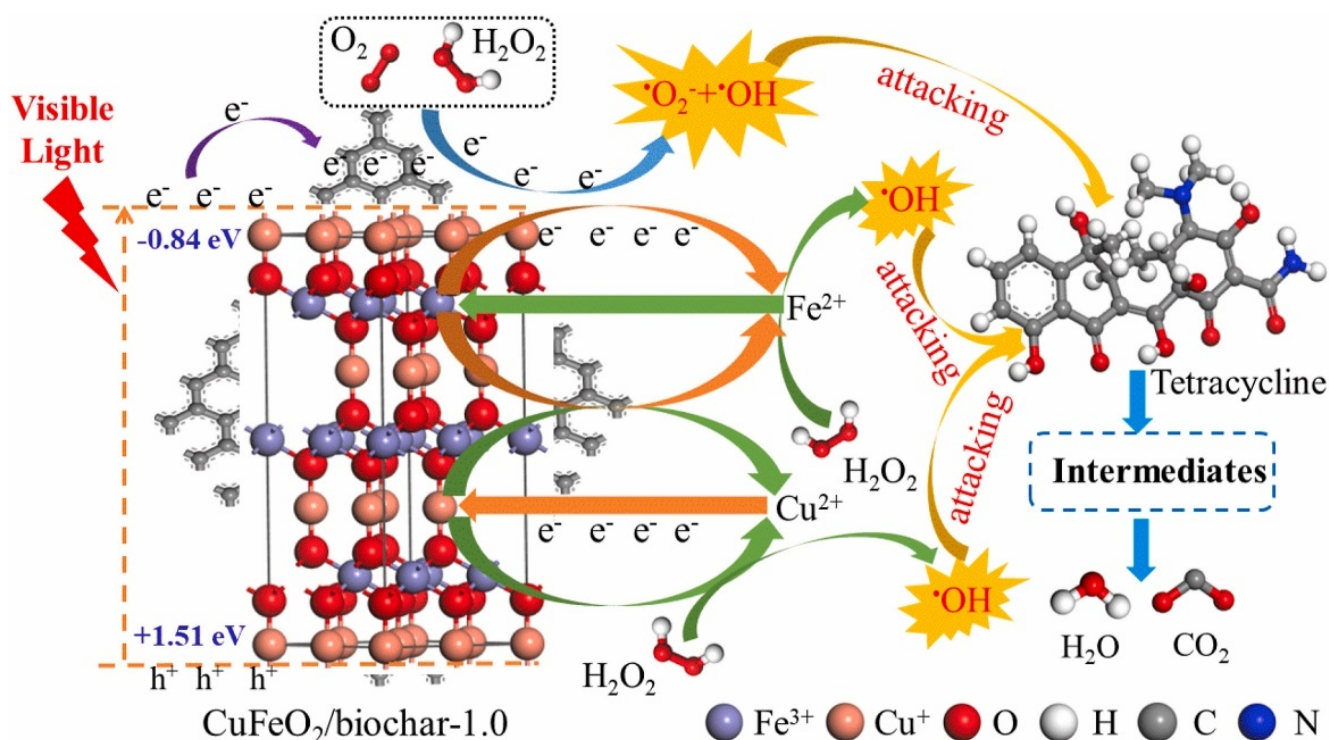


Figure 5. Possible mechanism of tetracycline degradation by $CuFeO_2$ /biochar in the heterogeneous photo-Fenton system. Reprinted with permission from Ref. [38]. Copyright 2020, Elsevier.

It is worth mentioning that the authors also explored the TC degradation intermediate products by HPLC-MS and proposed plausible transformation pathways. On the other hand, Xin et al. [91] also studied the heterogeneous visible-light Photo-electro-Fenton (H-VL-PEF) treatment of TC using an undivided photoelectrochemical cell in the presence of $CuFeO_2$ /biochar particles. A nitrogen/oxygen self-doped biomass porous carbon cathode was used as a gas diffusion electrode (GDE) to efficiently produce H_2O_2 , while a Xe-Lamp (filter > 420 nm) was used as a visible irradiation source for $CuFeO_2$ /biochar particles. The performances of different treatments (including electro-catalysis, photo-catalysis, photo-electro-catalysis, electro-Fenton, and H-VL-PEF) were evaluated for comparable experimental setups. The H-VL-PEF showed excellent performance, achieving the highest TC degradation rate and the best TOC removal with the lowest energy consumption. The authors analyzed the effect of several operational parameters and found that the full decomposition of TC (20 to 200 mg L^{-1}) was attained within 60–70 min under optimal conditions (i.e., 100 mg L^{-1} $CuFeO_2$ /biochar, 80 mA cm^{-2} of current density, and pH 5.0). Reutilization tests showed negligible metal leaching and small efficiency losses after 10 cycles. Experiments performed in the presence of selective scavengers of active species as well as ESR measurements indicated that HO^\bullet radicals are the main species responsible for TC degradation, whereas $O_2^{\bullet-}$ radicals play a subsidiary role. The schematic representation of the involved processes is presented in Figure 6. In addition, based on the intermediates detected by HPLC-MS analyses, the authors proposed general pathways for TC transformation and used a software tool for predicting, through QSAR techniques, the evolution of sample toxicity with the treatment time.

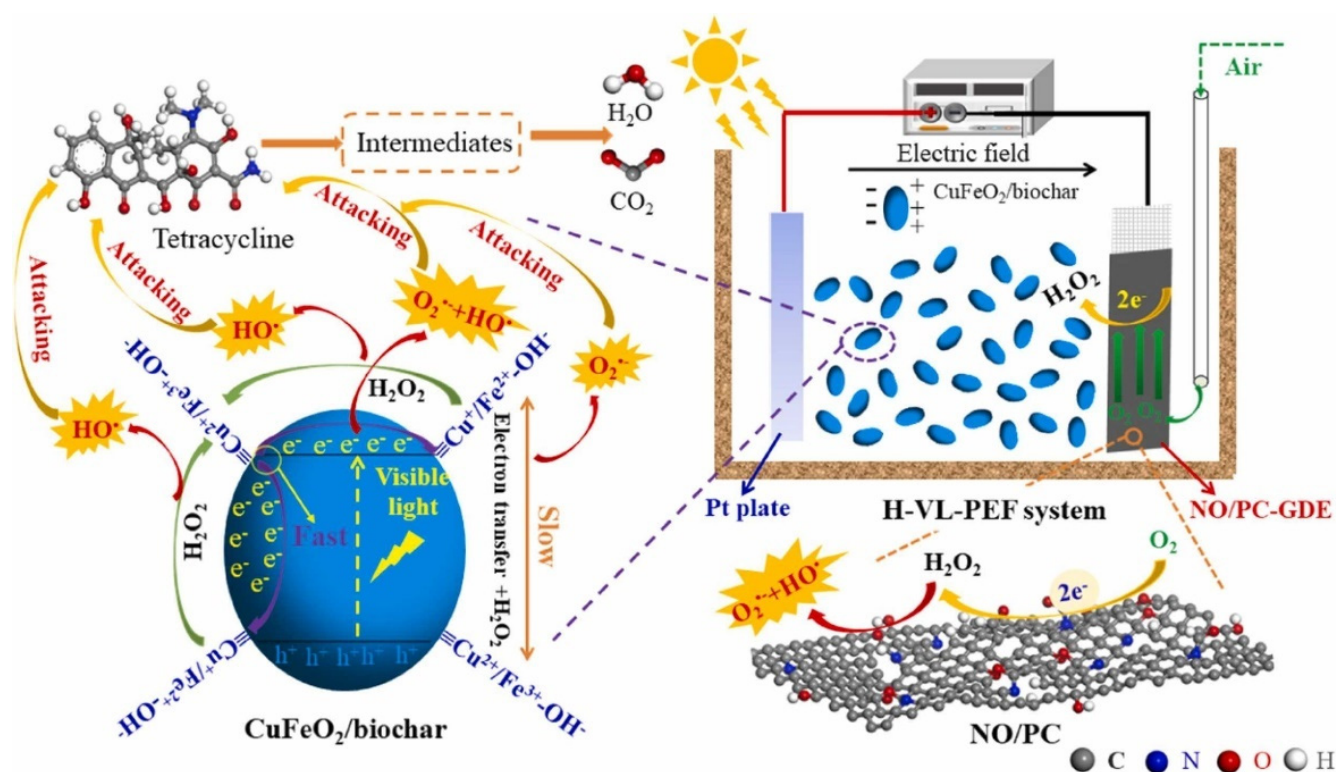


Figure 6. Possible mechanism of tetracycline degradation in the H-VL-PEF system. Reprinted with permission from Ref. [91]. Copyright 2020, Elsevier.

More recently, Xin et al. [92] achieved a further enhancement in the performance of photo-electro-Fenton (PEF) degradation of TC by introducing modifications to the latter treatment strategy. Three GDE composites were fabricated by mixing different weight ratios of a nitrogen/oxygen self-doped porous biochar (NO/PBC) cathode for H_2O_2 electrogeneration with a NO/PBC-supported $CuFeO_2$ ($CuFeO_2$ -NO/PBC) catalyst for H_2O_2 activation. The NO/PBC was prepared by the pyrolysis method, whereas $CuFeO_2$ -NO/PBC was prepared by the hydrothermal method without additional chemical reductants. The PEF treatment of TC was carried out in an undivided quartz reactor with a Pt anode and using visible light (Xe-Lamp, cutoff > 420 nm). The authors analyzed the effects of the NO/PBC to $CuFeO_2$ -NO/PBC ratio, the current density, and initial pH on system performance, which depends on the compromise between H_2O_2 formation, parallel reactions such as 4-electron oxygen reduction reaction (ORR) and H_2 evolution, and H_2O_2 decomposition. Using a NO/PBC to $CuFeO_2$ -NO/PBC ratio of 1:1, a current density of 80 mA cm^{-2} , and pH 5, an efficiency of 96.1% was achieved for TC (20 mg L^{-1}) degradation at 180 min in the PEF treatment. The latter value is twice the rate observed in EF and an order of magnitude higher than that recorded under anodic oxidation. The degradation efficiency at 180 min of PEF treatment steadily declined from 96.1% at pH 5.0 to 46.8% at pH 11.0. After five cycles of material use, the PEF treatment efficiency was higher than 80%, the amounts of leached Fe and Cu were negligible, and surface hydrophobicity remained practically constant. Assays in the presence of radical scavengers showed that HO^\bullet and $O_2^{\bullet-}$ played the primary and auxiliary roles for tetracycline degradation, respectively. The authors proposed that despite the photoinduced hole could not effectively participate in TC degradation, the photogenerated electrons reacted with H_2O_2 , O_2 , and Fe^{3+}/Cu^{2+} to form HO^\bullet , $O_2^{\bullet-}$, and Fe^{2+}/Cu^+ , respectively, thus promoting an efficient TC transformation. Finally, from the reaction intermediates detected by HPLC-MS, QSAR tools, and experiments of *E. coli* growth inhibition, a general picture of TC oxidation pathways and toxicity evolution was outlined.

All the results described in this section are summarized in Table 2.

Table 2. Summary of recently used $CuFeO_2$ and $CuFeS_2$ as photo-Fenton photocatalysts in wastewater treatment.

Material ^(a)	Conditions	Contaminant	Degradation Efficiency	Reference
Delafossite-type $CuFeO_2$ ^(b,c)	visible light, pH from 2.4 to 3.6, H_2O_2 from 3 to 13 mM, catalyst from 0.13 to 0.33 g L ⁻¹	Reactive Red 141 dye, 50 mg L ⁻¹	about 98% at 30 min	[86]
3R-delafossite $CuFeO_2$ microcrystals ^(b)	200 mL reactor, 20 mM of H_2O_2 , 1 g L ⁻¹ catalyst, initial pH 8	Tetracycline hydrochloride 20 mg L ⁻¹	96.1% in 180 min	[87]
$CuFeS_2$ ^(c)	visible light, 20 mM of H_2O_2 , 0.2 g L ⁻¹ catalyst, pH 6	bisphenol A (BPA) 20 mg L ⁻¹	97% in 60 min	[88]
$CuFeS_2$ chalcogenide powders ^(b,c)	visible light, pH 3.0, 8.33 mM of H_2O_2 , 0.2 g L ⁻¹ of catalyst	tartrazine, 100 mg L ⁻¹	99.1% of tartrazine decolorization after 40 min and 87.3% of mineralization after 150 min	[89]
MAMR-Fe-Cu@SiO ₂ /SC, a core-shell structure of $CuFeO_2$ @SiO ₂ /starch-derived carbon anchored on a Manganese Residue ^(d)	Xe-lamp with UV cut-off, pH from 2.5 to 9.5, 15 mM of H_2O_2 , 0.7 g L ⁻¹ of catalyst	Tetracycline 50 mg L ⁻¹	100% in 40 min	[90]
$CuFeO_2$ /biochar ^(b)	Xe Lamp with UV cutoff, pH 4 to 8, 20 mM of H_2O_2 , 0.2 g L ⁻¹ of catalyst	Tetracycline 20 mg L ⁻¹	97.6% in 120 min	[38]
$CuFeO_2$ /biochar ^(b)	photo-electro-Fenton, Xe-Lamp with UV cutoff, pH from 3 to 11, H_2O_2 generated by a NO-doped/porous carbon cathode	Tetracycline (20 to 200 mg L ⁻¹)	100% in 60–70 min	[91]
Nitrogen/oxygen self-doped porous biochar (NO/PBC) and NO/PBC-supported $CuFeO_2$ ($CuFeO_2$ -NO/PBC) ^(b)	undivided quartz reactor, visible light, pH from 3 to 11, H_2O_2 by a gas diffusion electrode	Tetracycline 20 mg L ⁻¹	98% at 30 min	[92]

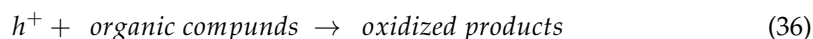
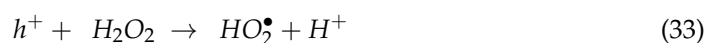
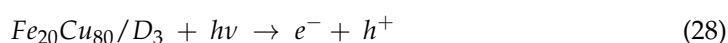
^(a) The synthesis method is shown in the footnotes. ^(b) Hydrothermal method. ^(c) Microwave-assisted hydrothermal method. ^(d) Reductive roasting and mechanical activation.

5. Fe–Cu Oxide Composites

In this section, we present the results obtained with other types of heterogeneous catalysts consisting of mixtures of iron and copper oxides and mixed oxides of defined composition. Heterojunctions formed by different copper and iron oxides and/or sulfides decrease the recombination rate of photogenerated e^- and h^+ [93,94].

Mansoori et al. [95] prepared an iron–copper oxide impregnated NaOH-activated biochar (Fe–Cu/ABC) through the pyrolysis of activated biochar, followed by the impregnation method. The catalytic activity of the bimetallic catalyst was tested for ciprofloxacin (CIP) degradation through a heterogeneous photo-electro-Fenton process) at a natural pH. The heterogeneous catalyst exhibited remarkable catalytic activity and showed great stability and structural integrity for five cycles. Furthermore, from a practical point of view, the catalyst exhibited an acceptable performance by oxidizing CIP dissolved in various water matrices such as tap water, river water, and a real sample of wastewater. The intermediates by-products of CIP were determined, and a plausible degradation mechanism was proposed. The adsorption of as-generated H_2O_2 onto the well-developed surface of the mesoporous bimetallic catalyst facilitated the reduction of Fe^{3+} to Fe^{2+} and Cu^{2+} to Cu^+ . The co-existence of Fe and Cu on the surface of activated biochar accelerates the process of electron transfer in the reaction and enhances the production of reactive species.

Iron oxide NPs supported on the surface of hydroxylated diamond exhibited photocatalytic activity and stability for the visible light-assisted Fenton reaction even working at pH values around 6 and demonstrated superiority as supports compared to other alternative solids such as activated carbon, graphite, carbon nanotubes, and even the benchmark semiconductor TiO_2 [96]. In particular, Manickam–Periyaraman, et al. [97] prepared bimetallic $Fe_{20}Cu_{80}$ NPs supported on various surface hydroxylated diamond NPs (D) and compared them to analogous catalysts based on graphite. The assays were conducted at pH 6 for the heterogeneous Fenton degradation of phenol (Ph) assisted by natural or simulated sunlight irradiation, achieving a mineralization degree of 90% at an H_2O_2 to Ph molar ratio of 6. The authors explained this result based on the high activity of reduced copper to form hydroxyl radicals and the favorable redox process of Fe^{2+} maintaining a pool of reduced Cu^+ species. Thus, a heterogeneous catalyst based on abundant iron or copper metals allowed the promotion of H_2O_2 activation to yield hydroxyl radicals under visible light irradiation according to Equations (28)–(36).



Khan et al. [98] compared the photocatalytic activity of novel peculiar-shaped CuO , Fe_2O_3 , and FeO nanoparticles (NPs) to that of the iron(II)-doped copper ferrite, $Cu^{II}_{0.4}Fe^{II}_{0.6}Fe^{III}_2O_4$, through the degradation of MB and RhB. The catalysts were synthesized via the simple co-precipitation and calcination technique. The highest degradation efficiency was achieved by CuO for RhB and by $Cu^{II}_{0.4}Fe^{II}_{0.6}Fe^{III}_2O_4$ for MB. The $CuO/FeO/Fe_2O_3$ composite proved to be the second-best catalyst in both cases, with excellent reusability.

Asenath–Smith et al. [99] used iron oxide (α - Fe_2O_3 , hematite) colloids synthesized under hydrothermal conditions as catalysts for the photodegradation of MO. To enhance the photocatalytic performance, Fe_2O_3 was combined with other transition-metal oxide (TMO) colloids (e.g., CuO and ZnO), which are sensitive to different regions of the solar spectrum (visible and UV, respectively), using a ternary blending approach for compositional mixtures. For a variety of $ZnO/Fe_2O_3/CuO$ mole ratios, the pseudo-first-order rate constant for MO degradation was at least twice the sum of the individual Fe_2O_3 and CuO rate constants, indicating that an underlying synergy governs the photocatalytic reactions for these combinations of TMOs. The increased photo-catalytic performance of Fe_2O_3 in the presence of CuO was associated with the hydroxyl radical, consistent with heterogeneous photo-Fenton mechanisms, which are not accessible by ZnO . Then, the authors proposed a mechanism where CuO plays a supportive role in Fe_2O_3 photocatalysis by decomposing H_2O_2 to generate HO^\bullet radicals. With additional ROS available, the reaction kinetics are accelerated. The bandgap energies of the TMOs used in this study further corroborated the obtained results. Smaller bandgap materials, such as Fe_2O_3 and CuO , have valence-band edges above the oxidation potential of H_2O . As a result, it is energetically favorable for a photogenerated h^+ on Fe_2O_3 or CuO to participate in the generation of HO^\bullet radicals by H_2O oxidation. Larger band gap materials, such as ZnO , have valence-band edges that are

below the H_2O oxidation potential for HO^\bullet formation, but their conduction band edges are below the reduction potential of O_2 .

Lu et al. [100] used a magnesium aluminum silicate known as attapulgite (ATP) supported $Fe-Mn-Cu$ polymetallic oxide as a catalyst with UV irradiation in the photo-catalytic oxidation (photo-Fenton) treatment of a synthetic pharmaceutical wastewater. $Fe-Mn-Cu@ATP$ had good catalytic potential and a significant synergistic effect since it removed almost all heterocyclic compounds, as well as humus-like and fulvic acid. The degradation efficiency of the nanocomposite only decreased by 5.8% after repeated use for six cycles (COD removal reached 64.9%, and the BOD_5/COD increased from 0.179 to 0.387 after 180 min of reaction time). The proposed mechanism involves: (i) the direct reaction between the catalyst and hydrogen peroxide, which generates HO^\bullet radicals and oxidized ions of the three metals, (ii) the UV photoreductions of these metal ions, and (iii) indirect reactions between photogenerated free radicals and the catalyst. In this mechanism, the consumed metal ions are effectively regenerated under UV light, and HO^\bullet finally reacts with the organic matter.

Davarnejad et al. [101] synthesized alginate-based hydrogel-coated bimetallic iron-copper nanocomposite beads through a green method and used them as heterogeneous catalysts for metronidazole elimination from wastewater. These authors employed the response surface methodology (RSM) based on the Box-Behnken design (BBD) to assess both the individual and interaction effects of five main variables involving catalyst loading, initial pH, reaction time, metronidazole, and H_2O_2 concentrations. The data obtained from the model were in good agreement with the experimental ones. The optimum conditions (for 95.3%, based on model, and for 95.0%, based on experiments) were found at a catalyst ($Fe_2O_3-CuO@Ca-Alg$) loading of 44.7 mg L^{-1} , an initial pH of 3.5, a metronidazole concentration of 10 mg L^{-1} , a H_2O_2 concentration of $33.17 \text{ mmol L}^{-1}$, and a reaction time of 85 min.

Zhang et al. [102] used $Fe_3O_4@Cu_2O$ /carbon quantum dots (CQDs)/nitrogen-doped carbon quantum dots (N-CQDs) (FCCN) for the degradation of azo compounds, such as MO, acid orange II, and mordant yellow 10, even at a neutral and alkaline pH (pH: 7–12) with a shortest time for complete degradation of 15 min. There is a cooperative interaction between each component, so the synergism from all the components of FCCN enhances the photocatalytic properties. The authors proposed a mechanism where in the first place, the up-conversion characteristics of CQDs and N-CQDs improve the light utilization of FCCN. Secondly, the load of CQDs and N-CQDs can separate and transfer photo-generated charges between Fe_3O_4 and Cu_2O more efficiently, accelerating the circulation of Fe^{3+}/Fe^{2+} for the decomposition of H_2O_2 to yield the active species: HO^\bullet radical. Thirdly, the light-induced protons of CQDs change the partial pH, so that the FCCN system is able to work in alkaline solutions. Finally, the insoluble layers of CQDs and N-CQDs are beneficial to enhance the stability of the composite (see in Figure 7 the schematic diagram of the catalytic mechanism proposed by the authors). The magnetism of Fe_3O_4 made this catalyst easily separable and the insoluble layers of CQDs and N-CQDs allowed it to be repeatedly used without activity change even after 10 cycles. The degradation rate constant of MO in the FCCN/ H_2O_2 /light system was 5.4 times higher than that of the $Fe_3O_4@Cu_2O/H_2O_2$ /light system, indicating that the loaded quantum dots greatly enhanced the photocatalytic activity. The degradation rate constant in the FCCN/ H_2O_2 /light system was 2.5 times higher than that of the simple mixture ($Fe_3O_4@Cu_2O + CQDs + N-CQDs$)/ H_2O_2 /light system, which suggests that these excellent catalytic performances should come from the synergism effect of all components in FCCN.

All the results described in this section are summarized in Table 3.

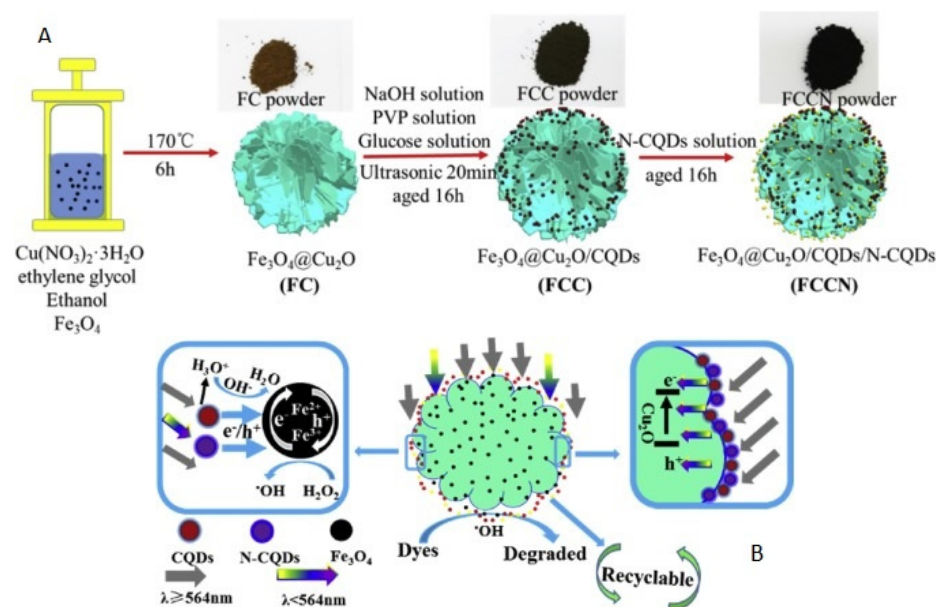


Figure 7. (A) Schematic illustration of the synthesis of FCCN. (B) Schematic diagram of the catalytic mechanism of FCCN (see text). Reprinted with permission from Ref. [91]. Copyright 2020, Elsevier.

Table 3. Summary of recently used *Fe–Cu* oxides composites as photo–Fenton photocatalysts in wastewater treatment.

Material ^(a)	Conditions	Contaminant	Degradation Efficiency	Reference
Iron–copper oxide impregnated <i>NaOH</i> -activated biochar (<i>FeCu/ABC</i> catalyst) ^(b)	Heterogeneous PEF process, pH = 5.8 catalyst dosage of 1 g L ⁻¹ , electrical current of 200 mA	CIP (45 mg L ⁻¹)	100% removal 2 h	[95]
<i>Fe</i> ₂₀ <i>Cu</i> ₈₀ (0.2 wt.%)/D3 ^(c)	catalyst ~200 mg L ⁻¹ , [H ₂ O ₂] (200 mg L ⁻¹ ; 5.88 mM), 20 °C, simulated sunlight. pH = 4	Phenol (100 mg L ⁻¹)	90% removal 2 h	[103]
NP-3 (<i>Cu</i> ^{II} 0.4 <i>Fe</i> ^{II} 0.6 <i>Fe</i> ^{III} 2 <i>O</i> ₄) ^(d)	NP-3 = 400 mg L ⁻¹ , [H ₂ O ₂] = 1.76 × 10 ⁻¹ mol L ⁻¹ , pH = 7.5 Optonica SP1275 LED lamp (GU10, 7 W, 400 Lm, 6000 K, Optonica LED, Sofia, Bulgaria)	MB (1.5 × 10 ⁻⁵ mol L ⁻¹) RhB (1.75 × 10 ⁻⁵ mol L ⁻¹)	100% 140 min	[98]
Iron oxide (α- <i>Fe</i> ₂ <i>O</i> ₃ , hematite) colloids combined with other transition–metal oxide (TMO) colloids (e.g., <i>CuO</i> and <i>ZnO</i>) ^(e)	750 mg L ⁻¹ catalyst, [H ₂ O ₂] = 0.025 mol L ⁻¹ . Tungsten halogen lamps	MO (25 μM)	7 to 78% 60 min	[99]
<i>Fe–Mn–Cu@ATP</i> ^(f)	500 mL of <i>Fe–Mn–Cu@ATP</i> dosage (1–12 g L ⁻¹), pH = 3 [H ₂ O ₂] (0.1–0.6 mol L ⁻¹) UV 40 W UV lamp	pharmaceutical wastewater	COD removal: 64.9% 180 min	[100]
<i>Fe</i> ₂ <i>O</i> ₃ – <i>CuO@Ca–Alg</i> hydrogel ^(g)	4.7 mg L ⁻¹ of catalyst, pH = 3.5 [H ₂ O ₂] = 33.17 mmol L ⁻¹ UV light	[MNZ] ₀ 10 mg L ⁻¹	Removal = 95% 85 min	[101]
FCCN ^(h)	Catalyst 1 g L ⁻¹ pH: 7–12 [H ₂ O ₂] = 15 mM 500W Xe lamp 564 nm cut-off filter	MO, acid orange II and mordant yellow 10–20 mg L ⁻¹	100% 15 min	[102]

^(a) The synthesis method is shown in the footnotes. ^(b) Pyrolysis of activated biochar followed by impregnation. ^(c) Deposition of the NPs (*Fe*, *Cu*, or *Fe–Cu*) onto the surface of commercial carbonaceous supports ^(d) Co-precipitation. ^(e) Hydrothermal method. ^(f) Aeration–coprecipitation method. ^(g) Green method using walnut green shells. ^(h) See Figure 7A.

6. Metal–Organic Frameworks Based on Fe and Cu

Metal–organic frameworks (MOFs) are inorganic–organic porous polymers composed of metal ions or metal clusters linked to each other by bridging organic ligands to form three-dimensional structures with a high specific surface area. In particular, Fe–based MOFs, made by polydentate organic ligands as linkers and inorganic Fe ions or Fe–oxo clusters as nodes, have recently attracted great attention in various applications such as gas adsorption, catalysis, and sensor development [104]. Within the applications, Fe–based MOFs have been considered promising catalysts in photo–Fenton processes due to their interfacial electron transfer properties and the cycling of the Fe(III)/Fe(II) redox pair. Additionally, the band gaps of Fe–based MOFs are suitable for visible light photoactivation and thus, Fe–O clusters could be directly excited to generate electron hole pairs ($e^- - h^+$), which subsequently degrade organic pollutants or lead to the generation of reactive oxygen species [105]. Likewise, it has been shown that the separation efficiency of photogenerated carriers in the Fe–O cluster remains low due to fast electron–hole recombination [105,106]. Taking this into account, different modifications in the structure of MOFs have been proposed to delay the recombination rate and improve pollutant degradation efficiencies [106,107]. In this sense, the combination of MOFs with metals or metal oxide nanoparticles may form a new interface or heterojunction that efficiently couples the catalytic process of photo–induced electrons and radicals' generation [108,109]. Moreover, the addition of a second metal ion into the nodes of frameworks could significantly improve the catalytic properties of MOFs [41]. Recently, different reports have incorporated Cu into Fe–based MOFs structure yielding Fe–Cu bimetallic MOFs in order to improve the performance of these materials in photo–Fenton processes.

Do et al. [110] reported the preparation of Fe–doped Cu 1,4–benzenedicarboxylate MOFs (Fe–CuBDC) and its application as a heterogeneous photo–Fenton catalyst for the degradation of MB in aqueous solution under visible light irradiation. In this work, the authors compared the efficiency of the bimetallic Fe–CuBDC with each single metal MOF. The degradation efficiency of MB with Fe–CuBDC was much higher than those obtained with the others, which indicates that the partial substitution of Cu by Fe significantly improves the photocatalytic activity of the material. Complete removal of MB was achieved after 70 min under light irradiation with 1.0 g L⁻¹ of Fe–CuBDC (Table 4). The degradation performance of the Fe–CuBDC catalyst was relatively constant with a slight reduction in removal efficiency from 99.9% to 97.2% after five reuse cycles.

Shi et al. [111] prepared a binary bimetallic heterojunction, which consisted of a core–shell magnetic CuFe₂O₄@MIL–100(Fe, Cu) metal–organic framework, via an in–situ derivation strategy. The synthesis methods, which involved the in situ surface pyrolysis of CuFe₂O₄ nanoparticles and complexation with trimesic acid to derive MIL–100(Fe, Cu), allowed the formation of a bimetallic core–shell CuFe₂O₄@MIL–100(Fe, Cu) heterojunction (MCuFe MOF). A schematic diagram of the synthesis process of MCuFe MOF is shown in Figure 8. These materials showed notable catalytic performance in a photo–Fenton process towards the degradation of various organic pollutants by increasing H₂O₂ activation efficiency and decreasing the required dosage of MCuFe MOF (0.05 g L⁻¹) over a wide pH range (4–9) (Table 4). Furthermore, the MCuFe MOF showed a high stability for the degradation of organic contaminants, with almost no decrease in activity and negligible metal leaching after five successive cycles. According to the proposed mechanism, the combination of the photothermal conversion effect with the formed heterojunction cannot only accelerate the generation and separation of photogenerated e^- and h^+ but also improve the continuous and efficient transformation of $\equiv\text{Fe(III)}/\text{Fe(II)}$ and $\equiv\text{Cu(II)}/\text{Cu(I)}$ redox couples, leading to enhanced photo–Fenton efficiency (see Figure 9).

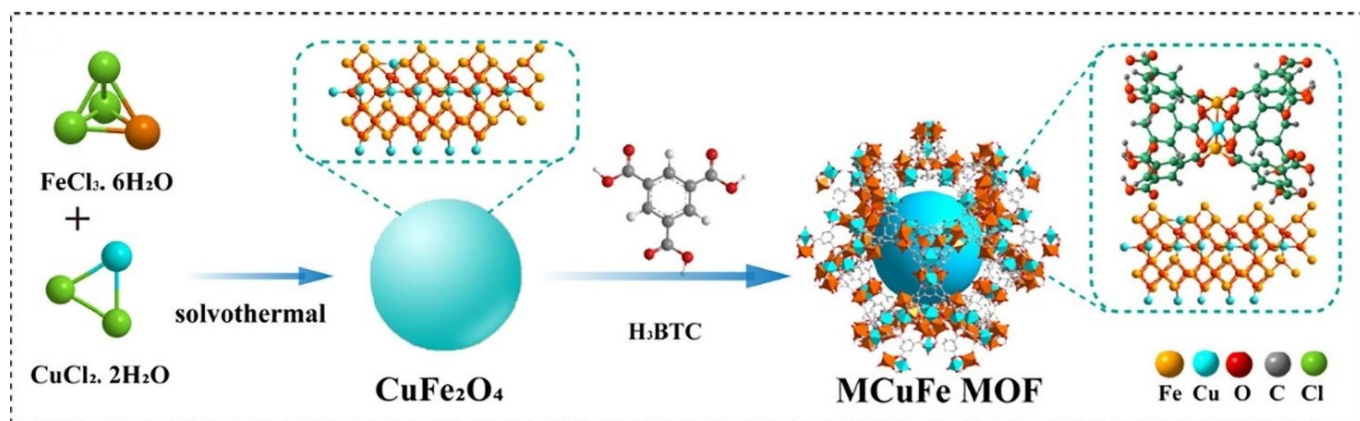


Figure 8. Schematic diagram of the synthesis process of *MCuFe* MOF. Reprinted with permission from Ref. [111]. Copyright 2020, Elsevier.

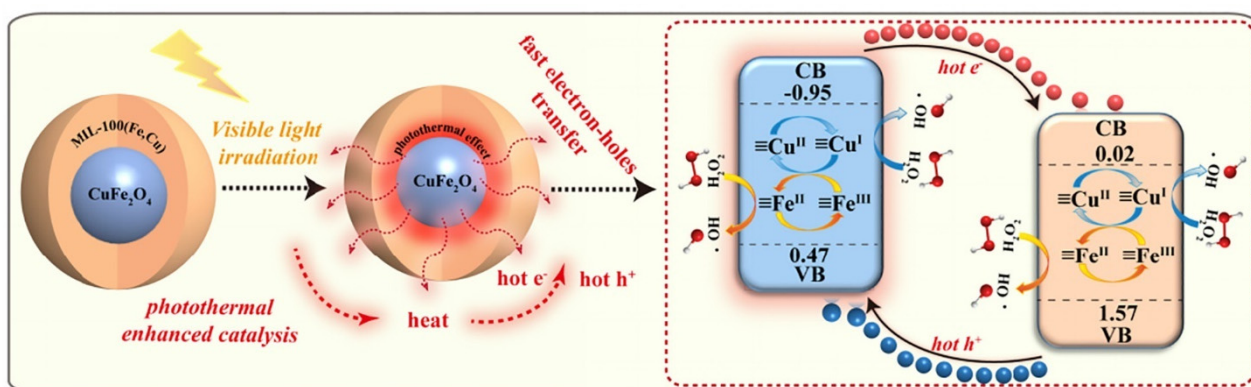


Figure 9. Photo-Fenton reaction mechanism of the charge transfer for hydroxyl radical generation over the *MCuFe* MOF under visible light irradiation. Reprinted with permission from Ref. [111]. Copyright 2020, Elsevier.

Table 4. Summary of recently used *Fe–Cu* bimetallic MOFs as photo-Fenton photocatalysts in wastewater treatment.

Material ^(a)	Conditions	Contaminant	Degradation Efficiency	Reference
<i>Fe–CuBDC</i> ^(b)	Simulated sunlight, pH 6, [H ₂ O ₂] = 50 mM, [Catalyst] = 1 g L ^{−1}	Methyl Blue (50 mg L ^{−1})	100% removal of the dye in 70 min	[110]
<i>MCuFe</i> MOF ^(b,c)	300 W xenon lamp equipped with a UV cut-off filter (λ > 400 nm), pH 4–9, [H ₂ O ₂] = 5 mM, [Catalyst] = 0.05 g L ^{−1}	Methyl Blue (50 mg L ^{−1})	100% removal of the dye in 40 min	[111]
<i>Cu₂O/MIL(Fe/Cu)</i> ^(b)	500 W xenon lamp, pH 7.47, [H ₂ O ₂] = 49 mM, [Catalyst] = 0.5 g L ^{−1}	Thiacloprid (80 mg L ^{−1})	100% removal of TCL in 20 min; 82% TOC removal in 80 min	[112]
<i>L–MIL–53 (Fe, Cu)</i> ^(b)	300 W xenon lamp equipped with a UV cut-off filter (λ > 420 nm), pH 7, [H ₂ O ₂] = 5 mM, [Catalyst] = 0.1 g L ^{−1}	Ciprofloxacin (20 mg L ^{−1})	60% removal of CIP in 30 min	[113]

^(a) The synthesis method is shown in the footnotes. ^(b) solvothermal method. ^(c) Hydrothermal method.

Zhong et al. [112] performed Cu_2O growth on the surface of Cu -doped MIL-100 (Fe) to obtain a $\text{Cu}_2\text{O}/\text{MIL}(\text{Fe}/\text{Cu})$ composite, which showed an enhanced interfacial synergistic effect and was successfully used as photo-Fenton catalysts for thiacloprid (TCL) degradation. The authors reported that Cu doping into $\text{MIL}(\text{Fe})$ led to the reduction in the band gap, and a boost of the redox cycle $\text{Fe}^{2+}/\text{Fe}^{3+}$. Likewise, the growth of Cu_2O extended the light absorption range of $\text{MIL}(\text{Fe}/\text{Cu})$ from UV to the visible region. A proposed TCL degradation mechanism is shown in Figure 10. $\text{Cu}_2\text{O}/\text{MIL}(\text{Fe}/\text{Cu})$ composite exhibited a TCL degradation rate nearly 10 times faster than those of Cu_2O and $\text{MIL-100}(\text{Fe})$, separately, achieving a complete TCL degradation within 20 min of reaction. Moreover, TOC removal reached 82.3% within 80 min under neutral conditions, which highlights the good performance of the $\text{Cu}_2\text{O}/\text{MIL}(\text{Fe}/\text{Cu})$ composite. Catalyst reuse tests showed no significant efficiency loss in reaction rates even after the tenth cycle, reaching complete TCL degradation within 20 min in each cycle.

Low-crystalline MOFs, with long-range disorder but local crystallinity, allow the availability of more active sites and defects than highly crystalline materials. These materials could improve the activation capacity of Fe -based MOFs towards H_2O_2 by increasing the number of metallic coordinately unsaturated active sites (CUS) within the frameworks. Wu et al. [113] prepared low-crystalline bimetallic MOFs of $\text{MIL-53}(\text{Fe}, \text{M})$ (M : Mn or Cu), via a one-pot solvothermal method, as photo-Fenton catalysts for the degradation of CIP. The results showed a significant improvement in photo-Fenton performance for the low-crystallinity catalyst compared to the crystalline counterparts, which was mainly attributed to the enhancement of the synergism between the hetero-metal nodes. In particular, low crystallinity $\text{MIL-53}(\text{Fe}, \text{Cu})$ exhibited a much higher removal efficiency and a faster reaction rate than that of crystalline $\text{MIL-53}(\text{Fe}, \text{Cu})$ within 30 min (Table 4). Besides the increased metal CUSs in the low-crystalline state, both Cu and Mn could increase the specific surface area and promote the visible-light absorption and separation/transportation of carriers in the low-crystalline state, thus leading to the acceleration of $\text{Fe}(\text{II})/\text{Fe}(\text{III})$ and $\text{M}(\text{red})/\text{M}(\text{ox})$ cycles.

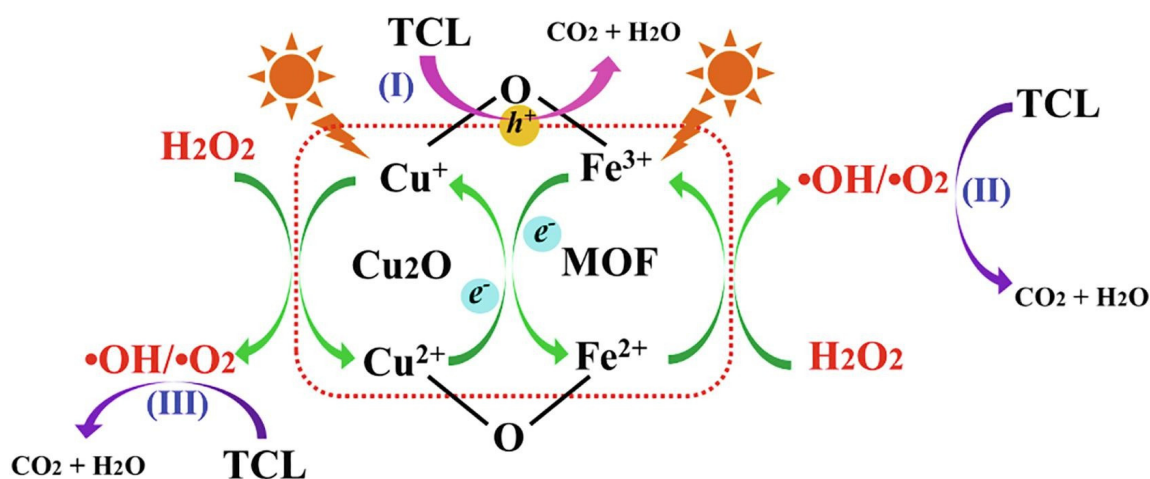


Figure 10. Proposed reaction mechanism for the photo-Fenton degradation of TCL over $\text{Cu}_2\text{O}/\text{MIL}(\text{Fe}/\text{Cu})$. Reprinted with permission from Ref. [112]. Copyright 2020, Elsevier.

All the results described in this section are summarized in Table 4.

7. Conclusions and Future Perspective

This review has shown the present trends in the development of bimetallic iron-copper materials and their application as catalysts in heterogeneous photo-Fenton-like reactions for the degradation of wastewater pollutants. Bimetallic Fe-Cu catalysts have shown better performance than monometallic Fe catalysts.

We have compared many materials with very different chemical compositions and physicochemical properties. In general, bimetallic *Fe–Cu* catalysts have shown better performance than monometallic *Fe* catalysts. In the works summarized here, it is difficult to find a common explanation of the synergistic effect of iron and copper on the catalytic activity of the materials. Some works attribute the improvement to changes in the band-gap, others to the decrease in the electron–hole recombination rates, and even to the reduction of H_2O_2 by electrons, or the beneficial effect of the binary redox couples of *Fe(II)/Fe(III)* and *Cu(I)/Cu(II)* on the decomposition efficiency of H_2O_2 . However, the common factor in all the materials seems to be that the coexistence of both metals evidently favors the redox cycles of *Fe* and *Cu*, resulting in higher catalytic activity. The co-existence of *Fe* and *Cu* on the surface of a catalyst accelerates the process of electron–transfer in the reaction environment, providing an appropriate condition for the activation of hydrogen peroxide and the generation of reactive radical species. This hypothesis is supported by the excellent degradation and mineralization results obtained when aqueous solutions of the contaminant are treated with these catalysts. In particular, lower degradation times and catalyst dosages are required to achieve complete pollutant degradation. Most of the bimetallic *Fe–Cu* catalysts have shown very good results at a circumneutral pH, which represents one of the major advantages of these materials since the development of an efficient and sustainable photo–Fenton treatment at neutral pH values remains a challenge for the scientific community working in the field. In addition, many of the works summarized here report the stability of the bimetallic catalysts even after having been used in four or five cycles.

From the analysis of the collected research, we can conclude that further efforts should focus on the preparation of new catalysts by green synthesis routes, that is, using bioactive agents such as plant materials, microorganisms, or biological waste. This approach would help to reduce the overall production cost and to limit environmental impact. Only a few of the compiled articles employed renewable energies such as natural solar light as the photoirradiation source. Most of them used either Xe lamps with or without cut–off filters for simulating sunlight or other light sources, such as UV lamps or visible light from lamps or LEDs. In this context, further studies devoted to addressing the effect of using solar light as the photoirradiation source on the performance of the catalysts are certainly encouraged.

Although excellent degradation and mineralization results have been obtained by applying this technique at the laboratory scale, its effectiveness needs to be evaluated in continuous flow systems for real industrial effluents. Most of the published research focused on the degradation of single pollutants (mainly dyes and antibiotics), disregarding the effects of the presence of humic–like dissolved organic matter and other contaminants. Moreover, to increase the efficiency and decrease the cost of the treatment of recalcitrant contaminants in real systems, the integration of photo–Fenton methods with biological technologies should be explored.

Author Contributions: Conceptualization, investigation, writing—original draft preparation, writing—review and editing: G.N.B., F.S.G.E., L.C. and D.O.M. contributed equally. All authors have read and agreed to the published version of the manuscript.

Funding: This project received funding from ANPCyT, Argentina (PICT 2017–1628, and PICT 2019–03140).

Data Availability Statement: Not applicable.

Acknowledgments: G.N. Bosio, F. García Einschlag, and L. Carlos and are staff researchers of CONICET (Argentina). D.O. Mártire is staff researcher of Comisión de Investigaciones Científicas (CIC, Buenos Aires, Argentina).

Conflicts of Interest: There are no conflicts of competing interest to declare.

References

1. Afrad, M.S.I.; Monir, M.B.; Haque, M.E.; Barau, A.A.; Haque, M.M. Impact of Industrial Effluent on Water, Soil and Rice Production in Bangladesh: A Case of Turag River Bank. *J. Environ. Health Sci. Eng.* **2020**, *18*, 825–834. [[CrossRef](#)] [[PubMed](#)]
2. Amor, C.; Marchão, L.; Lucas, M.S.; Peres, J.A. Application of Advanced Oxidation Processes for the Treatment of Recalcitrant Agro-Industrial Wastewater: A Review. *Water* **2019**, *11*, 205. [[CrossRef](#)]
3. Lama, G.; Meijide, J.; Sanromán, A.; Pazos, M. Heterogeneous Advanced Oxidation Processes: Current Approaches for Wastewater Treatment. *Catalysts* **2022**, *12*, 344. [[CrossRef](#)]
4. Shokri, A.; Fard, M.S. A Critical Review in Fenton-like Approach for the Removal of Pollutants in the Aqueous Environment. *Environ. Chall.* **2022**, *7*, 100534. [[CrossRef](#)]
5. Aparicio, F.; Escalada, J.P.; De Gerónimo, E.; Aparicio, V.C.; Einschlag, F.S.G.; Magnacca, G.; Carlos, L.; Mártire, D.O. Carbamazepine Degradation Mediated by Light in the Presence of Humic Substances-Coated Magnetite Nanoparticles. *Nanomaterials* **2019**, *9*, 1379. [[CrossRef](#)] [[PubMed](#)]
6. Litter, M.I.; Slodowicz, M. An Overview on Heterogeneous Fenton and PhotoFenton Reactions Using Zerovalent Iron Materials. *J. Adv. Oxid. Technol.* **2017**, *20*, 20160164. [[CrossRef](#)]
7. Babuponnusami, A.; Muthukumar, K. A Review on Fenton and Improvements to the Fenton Process for Wastewater Treatment. *J. Environ. Chem. Eng.* **2014**, *2*, 557–572. [[CrossRef](#)]
8. Bokare, A.D.; Choi, W. Review of Iron-Free Fenton-like Systems for Activating H₂O₂ in Advanced Oxidation Processes. *J. Hazard. Mater.* **2014**, *275*, 121–135. [[CrossRef](#)]
9. Hussain, S.; Aneghi, E.; Goi, D. Catalytic Activity of Metals in Heterogeneous Fenton-like Oxidation of Wastewater Contaminants: A Review. *Environ. Chem. Lett.* **2021**, *19*, 2405–2424. [[CrossRef](#)]
10. Nichela, D.A.; Berkovic, A.M.; Costante, M.R.; Juliarena, M.P.; García Einschlag, F.S. Nitrobenzene Degradation in Fenton-like Systems Using Cu(II) as Catalyst. Comparison between Cu(II)- and Fe(III)-Based Systems. *Chem. Eng. J.* **2013**, *228*, 1148–1157. [[CrossRef](#)]
11. Berkovic, A.M.; Costante, M.R.; García Einschlag, F.S. Combining Multivariate Curve Resolution and Lumped Kinetic Modelling for the Analysis of Lignin Degradation by Copper-Catalyzed Fenton-like Systems. *React. Chem. Eng.* **2022**, *7*, 1954–1967. [[CrossRef](#)]
12. Bali, U.; Karagözoğlu, B. Performance Comparison of Fenton Process, Ferric Coagulation and H₂O₂/Pyridine/Cu(II) System for Decolorization of Remazol Turquoise Blue G-133. *Dye Pigment.* **2007**, *74*, 73–80. [[CrossRef](#)]
13. Tian, X.; Jin, H.; Nie, Y.; Zhou, Z.; Yang, C.; Li, Y.; Wang, Y. Heterogeneous Fenton-like Degradation of Ofloxacin over a Wide PH Range of 3.6–10.0 over Modified Mesoporous Iron Oxide. *Chem. Eng. J.* **2017**, *328*, 397–405. [[CrossRef](#)]
14. Do, Q.C.; Kim, D.G.; Ko, S.O. Catalytic Activity Enhancement of a Fe₃O₄@SiO₂ Yolk-Shell Structure for Oxidative Degradation of Acetaminophen by Decoration with Copper. *J. Clean. Prod.* **2018**, *172*, 1243–1253. [[CrossRef](#)]
15. Salem, I.A. Kinetics of the Oxidative Color Removal and Degradation of Bromophenol Blue with Hydrogen Peroxide Catalyzed by Copper(II)-Supported Alumina and Zirconia. *Appl. Catal. B Environ.* **2000**, *28*, 153–162. [[CrossRef](#)]
16. Pignatello, J.; Oliveros, E.; MacKay, A. Advanced oxidation processes for organic contaminant destruction based on the fenton reaction and related chemistry. *Crit. Rev. Environ. Sci. Technol.* **2006**, *36*, 1–84. [[CrossRef](#)]
17. Zhang, M.H.; Dong, H.; Zhao, L.; Wang, D.-X.; Meng, D. A Review on Fenton Process for Organic Wastewater Treatment Based on Optimization Perspective. *Sci. Total Environ.* **2019**, *670*, 110–121. [[CrossRef](#)]
18. McNaught, A.D.; Wilkinson, A. *The IUPAC Compendium of Chemical Terminology*; International Union of Pure and Applied Chemistry (IUPAC): Durham, NC, USA, 2019; ISBN 0-9678550-9-8.
19. Sun, C.; Chen, C.; Ma, W.; Zhao, J. Photodegradation of Organic Pollutants Catalyzed by Iron Species under Visible Light Irradiation. *Phys. Chem. Chem. Phys.* **2011**, *13*, 1957–1969. [[CrossRef](#)] [[PubMed](#)]
20. Kalal, S.; Singh Chauhan, N.P.; Ameta, N.; Ameta, R.; Kumar, S.; Punjabi, P.B. Role of Copper Pyrovanadate as Heterogeneous Photo-Fenton like Catalyst for the Degradation of Neutral Red and Azure-B: An Eco-Friendly Approach. *Korean J. Chem. Eng.* **2014**, *31*, 2183–2191. [[CrossRef](#)]
21. Lee, H.J.; Lee, H.; Lee, C. Degradation of Diclofenac and Carbamazepine by the Copper(II)-Catalyzed Dark and Photo-Assisted Fenton-like Systems. *Chem. Eng. J.* **2014**, *245*, 258–264. [[CrossRef](#)]
22. Faust, B.C.; Hoigné, J. Photolysis of Fe (III)-Hydroxy Complexes as Sources of OH Radicals in Clouds, Fog and Rain. *Atmos. Environ. Part A Gen. Top.* **1990**, *24*, 79–89. [[CrossRef](#)]
23. Malato, S.; Fernández-Ibáñez, P.; Maldonado, M.I.; Blanco, J.; Gernjak, W. Decontamination and Disinfection of Water by Solar Photocatalysis: Recent Overview and Trends. *Catal. Today* **2009**, *147*, 1–59. [[CrossRef](#)]
24. García Einschlag, F.S.; Braun, A.M.; Oliveros, E. Fundamentals and Applications of the Photo-Fenton Process to Water Treatment. In *Handbook of Environmental Chemistry*; Springer: Berlin/Heidelberg, Germany, 2015; Volume 35, pp. 301–342.
25. Bauer, R.; Fallmann, H. The Photo-Fenton Oxidation—A Cheap and Efficient Wastewater Treatment Method. *Res. Chem. Intermed.* **1997**, *23*, 341–354. [[CrossRef](#)]
26. Pliego, G.; Zazo, J.A.; García-Muñoz, P.; Muñoz, M.; Casas, J.A.; Rodríguez, J.J. Trends in the Intensification of the Fenton Process for Wastewater Treatment: An Overview. *Crit. Rev. Environ. Sci. Technol.* **2015**, *45*, 2611–2692. [[CrossRef](#)]
27. Rahim Pouran, S.; Abdul Aziz, A.R.; Wan Daud, W.M.A. Review on the Main Advances in Photo-Fenton Oxidation System for Recalcitrant Wastewaters. *J. Ind. Eng. Chem.* **2015**, *21*, 53–69. [[CrossRef](#)]

28. Miralles–Cuevas, S.; Oller, I.; Pérez, J.A.S.; Malato, S. Application of Solar Photo–Fenton at Circumneutral PH to Nanofiltration Concentrates for Removal of Pharmaceuticals in MWTP Effluents. *Environ. Sci. Pollut. Res.* **2015**, *22*, 846–855. [[CrossRef](#)]
29. Maniakova, G.; Salmerón, I.; Aliste, M.; Inmaculada Polo–López, M.; Oller, I.; Malato, S.; Rizzo, L. Solar Photo–Fenton at Circumneutral PH Using Fe(III)–EDDS Compared to Ozonation for Tertiary Treatment of Urban Wastewater: Contaminants of Emerging Concern Removal and Toxicity Assessment. *Chem. Eng. J.* **2022**, *431*, 133474. [[CrossRef](#)]
30. López–Vincent, N.; Cruz–Alcalde, A.; Lai, C.; Giménez, J.; Esplugas, S.; Sans, C. Role of Sunlight and Oxygen on the Performance of Photo–Fenton Process at near Neutral PH Using Organic Fertilizers as Iron Chelates. *Sci. Total Environ.* **2022**, *803*, 149873. [[CrossRef](#)]
31. Ahile, U.J.; Wuana, R.A.; Itodo, A.U.; Sha’Ato, R.; Dantas, R.F. A Review on the Use of Chelating Agents as an Alternative to Promote Photo–Fenton at Neutral PH: Current Trends, Knowledge Gap and Future Studies. *Sci. Total Environ.* **2020**, *710*, 134872. [[CrossRef](#)]
32. Sanabria, P.; Wilde, M.L.; Ruiz–Padillo, A.; Sirtori, C. Trends in Fenton and Photo–Fenton Processes for Degradation of Antineoplastic Agents in Water Matrices: Current Knowledge and Future Challenges Evaluation Using a Bibliometric and Systematic Analysis. *Environ. Sci. Pollut. Res.* **2022**, *29*, 42168–42184. [[CrossRef](#)]
33. Matta, R.; Hanna, K.; Kone, T.; Chiron, S. Oxidation of 2,4,6-trinitrotoluene in the presence of different iron-bearing minerals at neutral pH. *Chem. Eng. J.* **2008**, *144*, 453–458. [[CrossRef](#)]
34. He, J.; Yang, X.; Men, B.; Wang, D. Interfacial Mechanisms of Heterogeneous Fenton Reactions Catalyzed by Iron–Based Materials: A Review. *J. Environ. Sci.* **2016**, *39*, 97–109. [[CrossRef](#)] [[PubMed](#)]
35. Zuo, S.; Jin, X.; Wang, X.; Lu, Y.; Zhu, Q.; Wang, J.; Liu, W.; Du, Y.; Wang, J. Sandwich Structure Stabilized Atomic Fe Catalyst for Highly Efficient Fenton–like Reaction at All PH Values. *Appl. Catal. B Environ.* **2021**, *282*, 119551. [[CrossRef](#)]
36. Xu, L.; Wang, J. Degradation of 2,4,6–Trichlorophenol Using Magnetic Nanoscaled Fe₃O₄/CeO₂ Composite as a Heterogeneous Fenton–like Catalyst. *Sep. Purif. Technol.* **2015**, *149*, 255–264. [[CrossRef](#)]
37. Wang, J.; Tang, J. Fe–Based Fenton–like Catalysts for Water Treatment: Catalytic Mechanisms and Applications. *J. Mol. Liq.* **2021**, *332*, 115755. [[CrossRef](#)]
38. Xin, S.; Ma, B.; Liu, G.; Ma, X.; Zhang, C.; Ma, X.; Gao, M.; Xin, Y. Enhanced Heterogeneous Photo–Fenton–like Degradation of Tetracycline over CuFeO₂/Biochar Catalyst through Accelerating Electron Transfer under Visible Light. *J. Environ. Manag.* **2021**, *285*, 112093. [[CrossRef](#)]
39. Wei, Y.; Wang, C.; Liu, D.; Jiang, L.; Chen, X.; Li, H.; Zhang, F. Photo–Catalytic Oxidation for Pyridine in Circumneutral Aqueous Solution by Magnetic Fe–Cu Materials Activated H₂O₂. *Chem. Eng. Res. Des.* **2020**, *163*, 1–11. [[CrossRef](#)]
40. Guo, X.; Xu, Y.; Wang, K.; Zha, F.; Tang, X.; Tian, H. Synthesis of Magnetic CuFe₂O₄ Self–Assembled Hollow Nanospheres and Its Application for Degrading Methylene Blue. *Res. Chem. Intermed.* **2020**, *46*, 853–869. [[CrossRef](#)]
41. Tang, J.; Wang, J. Iron–Copper Bimetallic Metal–Organic Frameworks for Efficient Fenton–like Degradation of Sulfamethoxazole under Mild Conditions. *Chemosphere* **2020**, *241*, 125002. [[CrossRef](#)]
42. Han, Z.; Dong, Y.; Dong, S. Copper–Iron Bimetal Modified PAN Fiber Complexes as Novel Heterogeneous Fenton Catalysts for Degradation of Organic Dye under Visible Light Irradiation. *J. Hazard. Mater.* **2011**, *189*, 241–248. [[CrossRef](#)]
43. Sun, Y.; Yang, Z.; Tian, P.; Sheng, Y.; Xu, J.; Han, Y.F. Oxidative Degradation of Nitrobenzene by a Fenton–like Reaction with Fe–Cu Bimetallic Catalysts. *Appl. Catal. B Environ.* **2019**, *244*, 1–10. [[CrossRef](#)]
44. Diodati, S.; Walton, R.I.; Mascotto, S.; Gross, S. Low–Temperature Wet Chemistry Synthetic Approaches towards Ferrites. *Inorg. Chem. Front.* **2020**, *7*, 3282–3314. [[CrossRef](#)]
45. Bastianello, M.; Gross, S.; Elm, M.T. Thermal Stability, Electrochemical and Structural Characterization of Hydrothermally Synthesised Cobalt Ferrite (CoFe₂O₄). *RSC Adv.* **2019**, *9*, 33282–33289. [[CrossRef](#)]
46. Ranga, R.; Kumar, A.; Kumari, P.; Singh, P.; Madaan, V.; Kumar, K. Ferrite Application as an Electrochemical Sensor: A Review. *Mater. Charact.* **2021**, *178*, 111269. [[CrossRef](#)]
47. Rana, G.; Dhiman, P.; Kumar, A.; Vo, D.V.N.; Sharma, G.; Sharma, S.; Naushad, M. Recent Advances on Nickel Nano–Ferrite: A Review on Processing Techniques, Properties and Diverse Applications. *Chem. Eng. Res. Des.* **2021**, *175*, 182–208. [[CrossRef](#)]
48. Kaur, B.; Kaushal, G.; Rana, S.; Kumar, P.; Khanra, P.; Dhiman, M. Magnetic Ferrites: A Brief Review About Substitution on Electric and Magnetic Properties. *ECS Trans.* **2022**, *107*, 9093–9101. [[CrossRef](#)]
49. Almessiere, M.A.; Slimani, Y.; Trukhanov, A.V.; Sadaqat, A.; Korkmaz, A.D.; Algarou, N.A.; Aydın, H.; Baykal, A.; Toprak, M.S. Review on Functional Bi–Component Nanocomposites Based on Hard/Soft Ferrites: Structural, Magnetic, Electrical and Microwave Absorption Properties. *Nano-Struct. Nano-Objects* **2021**, *26*, 100728. [[CrossRef](#)]
50. Chand, P.; Vaish, S.; Kumar, P. Structural, Optical and Dielectric Properties of Transition Metal (MFe₂O₄; M = Co, Ni and Zn) Nanoferrites. *Phys. B Condens. Matter* **2017**, *524*, 53–63. [[CrossRef](#)]
51. Kefeni, K.K.; Mamba, B.B. Photocatalytic Application of Spinel Ferrite Nanoparticles and Nanocomposites in Wastewater Treatment: Review. *Sustain. Mater. Technol.* **2020**, *23*, e00140. [[CrossRef](#)]
52. Shobana, M.K. Nanoferrites in Biosensors—A Review. *Mater. Sci. Eng. B Solid-State Mater. Adv. Technol.* **2021**, *272*, 115344. [[CrossRef](#)]
53. Amiri, M.; Salavati–Niasari, M.; Akbari, A. Magnetic Nanocarriers: Evolution of Spinel Ferrites for Medical Applications. *Adv. Colloid Interface Sci.* **2019**, *265*, 29–44. [[CrossRef](#)] [[PubMed](#)]

54. Alao, A.O.; Popoola, A.P.; Sanni, O. The Influence of Nanoparticle Inhibitors on the Corrosion Protection of Some Industrial Metals: A Review. *J. Bio-Tribo-Corrosion* **2022**, *8*, 68. [\[CrossRef\]](#)
55. Mmelesi, O.K.; Masunga, N.; Kuvarega, A.; Nkambule, T.T.; Mamba, B.B.; Kefeni, K.K. Cobalt Ferrite Nanoparticles and Nanocomposites: Photocatalytic, Antimicrobial Activity and Toxicity in Water Treatment. *Mater. Sci. Semicond. Process.* **2021**, *123*, 105523. [\[CrossRef\]](#)
56. Dippong, T.; Levei, E.A.; Cadar, O. Recent Advances in Synthesis and Applications of MFe_2O_4 ($M = Co, Cu, Mn, Ni, Zn$) Nanoparticles. *Nanomaterials* **2021**, *11*, 1560. [\[CrossRef\]](#)
57. Iqbal, M.J.; Yaqub, N.; Sepiol, B.; Ismail, B. A Study of the Influence of Crystallite Size on the Electrical and Magnetic Properties of $CuFe_2O_4$. *Mater. Res. Bull.* **2011**, *46*, 1837–1842. [\[CrossRef\]](#)
58. Bagade, A.; Nagwade, P.; Nagawade, A.; Thopate, S.; Pandit, V.; Pund, S. Impact of Mg^{2+} Substitution on Structural, Magnetic and Optical Properties of Cu–Cd Ferrites. *Mater. Today Proc.* **2022**, *53*, 144–152. [\[CrossRef\]](#)
59. Holinsworth, B.S.; Mazumdar, D.; Sims, H.; Sun, Q.C.; Yurtisigi, M.K.; Sarker, S.K.; Gupta, A.; Butler, W.H.; Musfeldt, J.L. Chemical Tuning of the Optical Band Gap in Spinel Ferrites: $CoFe_2O_4$ vs. $NiFe_2O_4$. *Appl. Phys. Lett.* **2013**, *103*, 082406. [\[CrossRef\]](#)
60. Lai, Y.J.; Lee, D.J. Solid Mediator Z–Scheme Heterojunction Photocatalysis for Pollutant Oxidation in Water: Principles and Synthesis Perspectives. *J. Taiwan Inst. Chem. Eng.* **2021**, *125*, 88–114. [\[CrossRef\]](#)
61. Feng, Y.; Lee, P.H.; Wu, D.; Zhou, Z.; Li, H.; Shih, K. Degradation of Contaminants by Cu^{+} -Activated Molecular Oxygen in Aqueous Solutions: Evidence for Cupryl Species (Cu^{3+}). *J. Hazard. Mater.* **2017**, *331*, 81–87. [\[CrossRef\]](#)
62. Silva, E.D.N.; Brasileiro, I.L.O.; Madeira, V.S.; De Farias, B.A.; Ramalho, M.L.A.; Rodríguez-Aguado, E.; Rodríguez-Castellón, E. Reusable $CuFe_2O_4$ – Fe_2O_3 catalyst Synthesis and Application for the Heterogeneous Photo–Fenton Degradation of Methylene Blue in Visible Light. *J. Environ. Chem. Eng.* **2020**, *8*, 104132. [\[CrossRef\]](#)
63. Cao, Z.; Zuo, C.; Wu, H. One Step for Synthesis of Magnetic $CuFe_2O_4$ Composites as Photo–Fenton Catalyst for Degradation Organics. *Mater. Chem. Phys.* **2019**, *237*, 121842. [\[CrossRef\]](#)
64. Leichtweis, J.; Silvestri, S.; Welter, N.; Vieira, Y.; Zaragoza–Sánchez, P.I.; Chávez–Mejía, A.C.; Carissimi, E. Wastewater Containing Emerging Contaminants Treated by Residues from the Brewing Industry Based on Biochar as a New $CuFe_2O_4$ /Biochar Photocatalyst. *Process Saf. Environ. Prot.* **2021**, *150*, 497–509. [\[CrossRef\]](#)
65. Jiang, J.; Gao, J.; Niu, S.; Wang, X.; Li, T.; Liu, S.; Lin, Y.; Xie, T.; Dong, S. Comparing Dark– and Photo–Fenton–like Degradation of Emerging Pollutant over Photo–Switchable $Bi_2WO_6/CuFe_2O_4$: Investigation on Dominant Reactive Oxidation Species. *J. Environ. Sci.* **2021**, *106*, 147–160. [\[CrossRef\]](#)
66. Clarizia, L.; Russo, D.; Di Somma, I.; Marotta, R.; Andreozzi, R. Homogeneous Photo–Fenton Processes at near Neutral PH: A Review. *Appl. Catal. B Environ.* **2017**, *209*, 358–371. [\[CrossRef\]](#)
67. Guo, X.; Wang, K.; Xu, Y. Tartaric Acid Enhanced $CuFe_2O_4$ –Catalyzed Heterogeneous Photo–Fenton–like Degradation of Methylene Blue. *Mater. Sci. Eng. B Solid-State Mater. Adv. Technol.* **2019**, *245*, 75–84. [\[CrossRef\]](#)
68. Li, Y.; Qin, C.; Zhang, J.; Lan, Y.; Zhou, L. $Cu(II)$ Catalytic Reduction of $Cr(VI)$ by Tartaric Acid under the Irradiation of Simulated Solar Light. *Environ. Eng. Sci.* **2014**, *31*, 447–452. [\[CrossRef\]](#) [\[PubMed\]](#)
69. Rocha, A.K.S.; Magnago, L.B.; Santos, J.J.; Leal, V.M.; Marins, A.A.L.; Pegoretti, V.C.B.; Ferreira, S.A.D.; Lelis, M.F.F.; Freitas, M.B.J.G. Copper Ferrite Synthesis from Spent Li–Ion Batteries for Multifunctional Application as Catalyst in Photo Fenton Process and as Electrochemical Pseudocapacitor. *Mater. Res. Bull.* **2019**, *113*, 231–240. [\[CrossRef\]](#)
70. Lin, Y.Y.; Lu, S.Y. Selective and Efficient Cleavage of Lignin Model Compound into Value–Added Aromatic Chemicals with $CuFe_2O_4$ Nanoparticles Decorated on Partially Reduced Graphene Oxides via Sunlight–Assisted Heterogeneous Fenton Processes. *J. Taiwan Inst. Chem. Eng.* **2019**, *97*, 264–271. [\[CrossRef\]](#)
71. Ayala, L.I.M.; Paquet, M.; Janowska, K.; Jamard, P.; Quist–Jensen, C.A.; Bosio, G.N.; Mártire, D.O.; Fabbri, D.; Boffa, V. Water Defluoridation: Nanofiltration vs. Membrane Distillation. *Ind. Eng. Chem. Res.* **2018**, *57*, 14740–14748. [\[CrossRef\]](#)
72. Wang, T.; Wang, Z.; Wang, P.; Tang, Y. An Integration of Photo–Fenton and Membrane Process for Water Treatment by a $PVDF@CuFe_2O_4$ Catalytic Membrane. *J. Membr. Sci.* **2019**, *572*, 419–427. [\[CrossRef\]](#)
73. Guin, D.; Baruwati, B.; Manorama, S.V. A Simple Chemical Synthesis of Nanocrystalline AFe_2O_4 ($A = Fe, Ni, Zn$): An Efficient Catalyst for Selective Oxidation of Styrene. *J. Mol. Catal. A Chem.* **2005**, *242*, 26–31. [\[CrossRef\]](#)
74. Zhenmin, L.; Xiaoyong, L.; Hong, W.; Dan, M.; Chaojian, X.; Dan, W. General Synthesis of Homogeneous Hollow Core–Shell Ferrite Microspheres. *J. Phys. Chem. C* **2009**, *113*, 2792–2797. [\[CrossRef\]](#)
75. Sharma, R.; Bansal, S.; Singhal, S. Tailoring the Photo–Fenton Activity of Spinel Ferrites (MFe_2O_4) by Incorporating Different Cations ($M = Cu, Zn, Ni$ and Co) in the Structure. *RSC Adv.* **2015**, *5*, 6006–6018. [\[CrossRef\]](#)
76. Li, N.; Fu, F.; Lu, J.; Ding, Z.; Tang, B.; Pang, J. Facile Preparation of Magnetic Mesoporous $MnFe_2O_4@SiO_2$ –CTAB Composites for $Cr(VI)$ Adsorption and Reduction. *Environ. Pollut.* **2017**, *220*, 1376–1385. [\[CrossRef\]](#)
77. Deng, J.; Xu, M.; Qiu, C.; Chen, Y.; Ma, X.; Gao, N.; Li, X. Magnetic $MnFe_2O_4$ Activated Peroxymonosulfate Processes for Degradation of Bisphenol A: Performance, Mechanism and Application Feasibility. *Appl. Surf. Sci.* **2018**, *459*, 138–147. [\[CrossRef\]](#)
78. Velinov, N.; Petrova, T.; Genova, I.; Ivanov, I.; Tsoncheva, T.; Idakiev, V.; Kunev, B.; Mitov, I. Synthesis and Mössbauer Spectroscopic Investigation of Copper–Manganese Ferrite Catalysts for Water–Gas Shift Reaction and Methanol Decomposition. *Mater. Res. Bull.* **2017**, *95*, 556–562. [\[CrossRef\]](#)
79. Fu, W.; Yi, J.; Cheng, M.; Liu, Y.; Zhang, G.; Li, L.; Du, L.; Li, B.; Wang, G.; Yang, X. When Bimetallic Oxides and Their Complexes Meet Fenton–like Process. *J. Hazard. Mater.* **2022**, *424*, 127419. [\[CrossRef\]](#) [\[PubMed\]](#)

80. Meena, S.; Anantharaju, K.S.; Vidya, Y.S.; Renuka, L.; Uma, B.; Sharma, S.C.; Prasad, B.D.; More, S.S. Enhanced Sunlight Driven Photocatalytic Activity and Electrochemical Sensing Properties of Ce-Doped MnFe_2O_4 Nano Magnetic Ferrites. *Ceram. Int.* **2021**, *47*, 14760–14774. [[CrossRef](#)]
81. Niu, J.; Qian, H.; Liu, J.; Liu, H.; Zhang, P.; Duan, E. Process and Mechanism of Toluene Oxidation Using $\text{Cu}_{1-y}\text{Mn}_2\text{Ce}_y\text{O}_x$ /Sepiolite Prepared by the Co-Precipitation Method. *J. Hazard. Mater.* **2018**, *357*, 332–340. [[CrossRef](#)] [[PubMed](#)]
82. Sun, Y.; Zhou, J.; Liu, D.; Li, X.; Liang, H. Enhanced Catalytic Performance of Cu-Doped MnFe_2O_4 Magnetic Ferrites: Tetracycline Hydrochloride Attacked by Superoxide Radicals Efficiently in a Strong Alkaline Environment. *Chemosphere* **2022**, *297*, 134154. [[CrossRef](#)]
83. Yang, J.; Zhang, Y.; Zeng, D.; Zhang, B.; Hassan, M.; Li, P.; Qi, C.; He, Y. Enhanced Catalytic Activation of Photo-Fenton Process by $\text{Cu}_{0.5}\text{Mn}_{0.5}\text{Fe}_2\text{O}_4$ for Effective Removal of Organic Contaminants. *Chemosphere* **2020**, *247*, 125780. [[CrossRef](#)] [[PubMed](#)]
84. Wang, X.T.; Li, Y.; Zhang, X.Q.; Li, J.F.; Luo, Y.N.; Wang, C.W. Fabrication of a Magnetically Separable $\text{Cu}_2\text{ZnSnS}_4/\text{ZnFe}_2\text{O}_4$ p-n Heterostructured Nano-Photocatalyst for Synergistic Enhancement of Photocatalytic Activity Combining with Photo-Fenton Reaction. *Appl. Surf. Sci.* **2019**, *479*, 86–95. [[CrossRef](#)]
85. Shi, L.; Shi, Y.; Zhuo, S.; Zhang, C.; Aldrees, Y.; Aleid, S.; Wang, P. Multi-Functional 3D Honeycomb Ceramic Plate for Clean Water Production by Heterogeneous Photo-Fenton Reaction and Solar-Driven Water Evaporation. *Nano Energy* **2019**, *60*, 222–230. [[CrossRef](#)]
86. Schmachtenberg, N.; Silvestri, S.; Da Silveira Salla, J.; Dotto, G.L.; Hotza, D.; Jahn, S.L.; Foletto, E.L. Preparation of Delafossite-Type CuFeO_2 Powders by Conventional and Microwave-Assisted Hydrothermal Routes for Use as Photo-Fenton Catalysts. *J. Environ. Chem. Eng.* **2019**, *7*, 102954. [[CrossRef](#)]
87. Liu, Q.L.; Zhao, Z.Y.; Zhao, R.D.; Yi, J.H. Fundamental Properties of Delafossite CuFeO_2 as Photocatalyst for Solar Energy Conversion. *J. Alloys Compd.* **2020**, *819*, 153032. [[CrossRef](#)]
88. da Silveira Salla, J.; da Boit Martinello, K.; Dotto, G.L.; García-Díaz, E.; Javed, H.; Alvarez, P.J.J.; Foletto, E.L. Synthesis of Citrate-Modified CuFeS_2 Catalyst with Significant Effect on the Photo-Fenton Degradation Efficiency of Bisphenol a under Visible Light and near-Neutral PH. *Colloids Surfaces A Physicochem. Eng. Asp.* **2020**, *595*, 124679. [[CrossRef](#)]
89. Da Silveira Salla, J.; Dotto, G.L.; Hotza, D.; Landers, R.; Da Boit Martinello, K.; Foletto, E.L. Enhanced Catalytic Performance of CuFeS_2 chalcogenide Prepared by Microwave-Assisted Route for Photo-Fenton Oxidation of Emerging Pollutant in Water. *J. Environ. Chem. Eng.* **2020**, *8*, 104077. [[CrossRef](#)]
90. Cai, X.; Huang, Q.; Hong, Z.; Zhang, Y.; Hu, H.; Huang, Z.; Liang, J.; Qin, Y. Cu Anchored on Manganese Residue through Mechanical Activation to Prepare a Fe-Cu@ SiO_2 /Starch-Derived Carbon Composites with Highly Stable and Active Visible Light Photocatalytic Performance. *J. Environ. Chem. Eng.* **2021**, *9*, 104710. [[CrossRef](#)]
91. Xin, S.; Huo, S.; Zhang, C.; Ma, X.; Liu, W.; Xin, Y.; Gao, M. Coupling Nitrogen/Oxygen Self-Doped Biomass Porous Carbon Cathode Catalyst with CuFeO_2 /Biochar Particle Catalyst for the Heterogeneous Visible-Light Driven Photo-Electro-Fenton Degradation of Tetracycline. *Appl. Catal. B Environ.* **2022**, *305*, 121024. [[CrossRef](#)]
92. Xin, S.; Huo, S.; Xin, Y.; Gao, M.; Wang, Y.; Liu, W.; Zhang, C.; Ma, X. Heterogeneous Photo-Electro-Fenton Degradation of Tetracycline through Nitrogen/Oxygen Self-Doped Porous Biochar Supported CuFeO_2 Multifunctional Cathode Catalyst under Visible Light. *Appl. Catal. B Environ.* **2022**, *312*, 121442. [[CrossRef](#)]
93. Aparicio, F.; Mizrahi, M.; Ramallo-López, J.M.; Laurenti, E.; Magnacca, G.; Carlos, L.; Mártire, D.O. Novel Bimetallic Magnetic Nanocomposites Obtained from Waste-Sourced Bio-Based Substances as Sustainable Photocatalysts. *Mater. Res. Bull.* **2022**, *152*, 111846. [[CrossRef](#)]
94. Ayala, L.I.M.; Aparicio, F.; Boffa, V.; Magnacca, G.; Carlos, L.; Bosio, G.N.; Mártire, D.O. Removal of As(III) via Adsorption and Photocatalytic Oxidation with Magnetic Fe-Cu Nanocomposites. *Photochem. Photobiol. Sci.* **2022**, *1*, 1–10. [[CrossRef](#)]
95. Mansoori, S.; Davarnejad, R.; Ozumchelouei, E.J.; Ismail, A.F. Activated Biochar Supported Iron-Copper Oxide Bimetallic Catalyst for Degradation of Ciprofloxacin via Photo-Assisted Electro-Fenton Process: A Mild PH Condition. *J. Water Process Eng.* **2021**, *39*, 101888. [[CrossRef](#)]
96. Espinosa, J.C.; Catalá, C.; Navalón, S.; Ferrer, B.; Álvaro, M.; García, H. Iron Oxide Nanoparticles Supported on Diamond Nanoparticles as Efficient and Stable Catalyst for the Visible Light Assisted Fenton Reaction. *Appl. Catal. B Environ.* **2018**, *226*, 242–251. [[CrossRef](#)]
97. Manickam-Periyaraman, P.; Espinosa, J.C.; Ferrer, B.; Subramanian, S.; Álvaro, M.; García, H.; Navalón, S. Bimetallic Iron-Copper Oxide Nanoparticles Supported on Nanometric Diamond as Efficient and Stable Sunlight-Assisted Fenton Photocatalyst. *Chem. Eng. J.* **2020**, *393*, 124770. [[CrossRef](#)]
98. Khan, A.; Valicsek, Z.; Horváth, O. Comparing the Degradation Potential of Copper(II), Iron(II), Iron(III) Oxides, and Their Composite Nanoparticles in a Heterogeneous Photo-Fenton System. *Nanomaterials* **2021**, *11*, 225. [[CrossRef](#)]
99. Asenath-Smith, E.; Ambrogi, E.K.; Barnes, E.; Brame, J.A. CuO Enhances the Photocatalytic Activity of Fe_2O_3 through Synergistic Reactive Oxygen Species Interactions. *Colloids Surfaces A Physicochem. Eng. Asp.* **2020**, *603*, 125179. [[CrossRef](#)]
100. Lu, M.; Wang, J.; Wang, Y.; He, Z. Heterogeneous Photo-Fenton Catalytic Degradation of Practical Pharmaceutical Wastewater by Modified Attapulgite Supported Multi-Metal Oxides. *Water* **2021**, *13*, 156. [[CrossRef](#)]
101. Davarnejad, R.; Hassanvand, Z.R.; Mansoori, S.; Kennedy, J.F. Metronidazole Elimination from Wastewater through Photo-Fenton Process Using Green-Synthesized Alginate-Based Hydrogel Coated Bimetallic Iron-copper Nanocomposite Beads as a Reusable Heterogeneous Catalyst. *Bioresour. Technol. Rep.* **2022**, *18*, 101068. [[CrossRef](#)]

102. Zhang, Y.; Guo, P.; Jin, M.; Gao, G.; Xi, Q.; Zhou, H.; Xu, G.; Xu, J. Promoting the Photo-Fenton Catalytic Activity with Carbon Dots: Broadening Light Absorption, Higher Applicable PH and Better Reuse Performance. *Mol. Catal.* **2020**, *481*, 110254. [[CrossRef](#)]
103. Zhang, B.; Hou, Y.; Yu, Z.; Liu, Y.; Huang, J.; Qian, L.; Xiong, J. Three-Dimensional Electro-Fenton Degradation of Rhodamine B with Efficient Fe-Cu/Kaolin Particle Electrodes: Electrodes Optimization, Kinetics, Influencing Factors and Mechanism. *Sep. Purif. Technol.* **2019**, *210*, 60–68. [[CrossRef](#)]
104. Joseph, J.; Iftexhar, S.; Srivastava, V.; Fallah, Z.; Zare, E.N.; Sillanpää, M. Iron-Based Metal-Organic Framework: Synthesis, Structure and Current Technologies for Water Reclamation with Deep Insight into Framework Integrity. *Chemosphere* **2021**, *284*, 131171. [[CrossRef](#)] [[PubMed](#)]
105. Wang, D.; Wang, M.; Li, Z. Fe-Based Metal-Organic Frameworks for Highly Selective Photocatalytic Benzene Hydroxylation to Phenol. *ACS Catal.* **2015**, *5*, 6852–6857. [[CrossRef](#)]
106. Ahmad, M.; Chen, S.; Ye, F.; Quan, X.; Afzal, S.; Yu, H.; Zhao, X. Efficient Photo-Fenton Activity in Mesoporous MIL-100(Fe) Decorated with ZnO Nanosphere for Pollutants Degradation. *Appl. Catal. B Environ.* **2019**, *245*, 428–438. [[CrossRef](#)]
107. He, X.; Fang, H.; Gosztola, D.J.; Jiang, Z.; Jena, P.; Wang, W.N. Mechanistic Insight into Photocatalytic Pathways of MIL-100(Fe)/TiO₂ Composites. *ACS Appl. Mater. Interfaces* **2019**, *11*, 12516–12524. [[CrossRef](#)] [[PubMed](#)]
108. Oladipo, A.A. MIL-53 (Fe)-Based Photo-Sensitive Composite for Degradation of Organochlorinated Herbicide and Enhanced Reduction of Cr(VI). *Process Saf. Environ. Prot.* **2018**, *116*, 413–423. [[CrossRef](#)]
109. Wang, Q.; Gao, Q.; Al-Enizi, A.M.; Nafady, A.; Ma, S. Recent Advances in MOF-Based Photocatalysis: Environmental Remediation under Visible Light. *Inorg. Chem. Front.* **2020**, *7*, 300–339. [[CrossRef](#)]
110. Do, T.L.; Ho, T.M.T.; Doan, V.D.; Le, V.T.; Hoai Thuong, N. Iron-Doped Copper 1,4-Benzenedicarboxylate as Photo-Fenton Catalyst for Degradation of Methylene Blue. *Toxicol. Environ. Chem.* **2019**, *101*, 13–25. [[CrossRef](#)]
111. Shi, S.; Han, X.; Liu, J.; Lan, X.; Feng, J.; Li, Y.; Zhang, W.; Wang, J. Photothermal-Boosted Effect of Binary Cu-Fe Bimetallic Magnetic MOF Heterojunction for High-Performance Photo-Fenton Degradation of Organic Pollutants. *Sci. Total Environ.* **2021**, *795*, 148883. [[CrossRef](#)]
112. Zhong, Z.; Li, M.; Fu, J.; Wang, Y.; Muhammad, Y.; Li, S.; Wang, J.; Zhao, Z.; Zhao, Z. Construction of Cu-Bridged Cu₂O/MIL(Fe/Cu) Catalyst with Enhanced Interfacial Contact for the Synergistic Photo-Fenton Degradation of Thiocloprid. *Chem. Eng. J.* **2020**, *395*, 125184. [[CrossRef](#)]
113. Wu, Q.; Siddique, M.S.; Guo, Y.; Wu, M.; Yang, Y.; Yang, H. Low-Crystalline Bimetallic Metal-Organic Frameworks as an Excellent Platform for Photo-Fenton Degradation of Organic Contaminants: Intensified Synergism between Hetero-Metal Nodes. *Appl. Catal. B Environ.* **2021**, *286*, 119950. [[CrossRef](#)]

Disclaimer/Publisher's Note: The statements, opinions and data contained in all publications are solely those of the individual author(s) and contributor(s) and not of MDPI and/or the editor(s). MDPI and/or the editor(s) disclaim responsibility for any injury to people or property resulting from any ideas, methods, instructions or products referred to in the content.